Notas de Física - Volume XIII - Nº 4

OBSERVATION OF EXTREMELY HIGH ENERGY NUCLEAR INTERACTIONS WITH EMULSION CHAMBER

M. Akashi, Z. Watanabe
Hirosaki University

K. Nishikawa, Y. Oyama, S. Hazama
Konan University

K. Ogata, T. Tsuneoka, T. Shirai
Kwansei Gakuin University

A. Nishio
Kyoto University

I. Mito, K. Niu, I. Ohta, T. Taira
The Institute for Nuclear Study, University of Tokyo

J. Nishimura
The Institute of Space and Aeronautical Science
University of Tokyo

N. Ogita
The Institute of Phys. and Chem. Research

Y. Fujimoto, S. Hasegawa, A. Osawa, T. Shibata
Waseda University

Y. Maeda
Yokohama National University

C. M. G. Lattes, N. Amato, V. D. Ferreira, C. Aguirre
Centro Brasileiro de Pesquisas Físicas, Rio de Janeiro

M. S. Mantovani, C. Santos, M. Schönberg
Universidade de São Paulo, São Paulo

(Received July 12, 1967)

The present report covers experimental results obtained by the emulsion chambers exposed at Mt. Chacaltaya (5.200 m), Bolivia and Mt. Norikura (2.800 m), Japan. Table A presents a list of the exposures, made up to the present.

Design of the Producer Chamber (Exposed from May 10^{th} 1965 to April 4^{th} 1966).

The present chamber was designed to observe in detail the jet showers produced in the chamber itself. The chamber consists of three parts as shown in Fig. 1, which are called as upper chamber, producing layer and lower chamber, respectively.

The upper chamber consists of 8 cm Pb plates and 4 nuclear emulsion layers. The γ-rays from the atmosphere are observed in this part and they are absorbed almost completely during their passage there. The producing layer is 70 g/cm^2 thick of petrolium pitch and is placed just under the upper chamber. The lower chamber consists of 20 cm lead plates and 13 emulsion layers.

Detection and Classification of the Events

The upper chamber detects particles coming directly from the atmosphere, mainly being composed of high energy γ-rays and electrons of atmospheric origin.

For all the events detected in the lower chamber, their arrival directions were measured by following through the neighbouring emulsion plates and they are classified by geometrical consideration whether their incident particles pass through the upper chamber or not. We select for further measurements only

those whose incident particles pass through the upper chamber. They are not cascade showers caused by γ-rays (nor electrons either) of atmospheric origin, but mainly the nuclear interactions caused either in the producing layers or in the chamber.

C-jets and Pb-jets

The selected events in the lower chamber is further classified into two groups: the interaction events caused in the producing layer (C-jets) and those in the chamber itself Pb-jets). This discrimination is possible without any ambiguity because of presence of spacing of 85 cm between the producer and the lower chamber.

In practice, careful microscopic scanning is made in nuclear emulsion plates at 4, 6 and 8 cascade unit over an area of radius 1.5 mm around the event. When one finds associated showers there showing multi-core structure of the events, they are assigned as C-jets. In this way, cores of C-jets with energy above 250 GeV can be detected without any bias.

PART I - FLUX MEASUREMENTS

The γ-Ray Spectrum

Atmospheric γ-rays (and electrons) are detected in the upper chamber and their energies are estimated by photo-metric measurement on the spots in the X-ray film. The "single" γ-ray spectrum are obtained eliminating fluctuation effect from γ-ray families.

The result is presented in Fig. 2. It can be expressed as the

absolute vertical flux being.

$$S_2(E_\gamma \geq 3 \text{ TeV}) = (1.2 \pm 0.2) \times 10^{-10}/\text{cm}^2 \text{ sec sterad},$$

and exponent of the power spectrum being,

$$\beta = 2.0 \pm 0.3.$$

Details of the measuring method and definition of the "single" spectrum, $S_2(E)$, were reported at the London Conference [2, 3]. The present results are in agreement with our previous measurement.[2,3]

The N-Particle Spectrum

The depth distribution of starting point of Pb-jets in the lower chamber allows us to estimate of nuclear collision mean free path of N-particles, as $\lambda_N = 191 \pm 29$ g cm^2(see Fig. 3). The production rate of nuclear interactions is obtained from the observed frequency of Pb-jet after making correction for absorption in the upper chamber and the producing layer. The energy spectrum of the N-particle is now obtained as the absolute value being,

$$I_N(E_\gamma \geq 3 \text{ TeV}) = (4.3 \pm 0.5)\ 10^{-10}/\text{cm}^2 \text{ sec sterad},$$

where $\sum E_\gamma$ is the total energy converted into γ-rays in the interaction, and exponent of the power being

$$\beta_N = 1.9 \pm 0.3$$

Figure 4 shows the spectrum. This is also consistent with our previous result reported at the London Conference [2, 3].

Production Rate of C-Jets

Energy measurement is made for all sub-cores of C-jets by the track counting method. The total radiated energy $\sum E_\gamma$ is obtain

ed by adding energies of the sub-cores. Some of C-jets suffer by chance cascade degradation during their passage through the producing layer. In these cases, the above method can not be applied for the energy estimation and the photo-metric method is used to estimate $\sum E_\gamma$.

Observed energy spectrum of C-jets is presented in Fig. 5. Its absolute value and slope of the spectrum agrees well with those obtained from Pb-jets, showing no serious detection bias for C-jets with $\sum E_\gamma \geq 3$ TeV.

PART II - C-JETS

The P_T-Distribution

Table II shows the number of observed C-jets which are included in the following analysis on the fire ball. Here the criterion of selection is that the observed total energy $\sum E_\gamma$ is larger than 3 TeV and they suffer practically no cascade degradation during their passage through the carbon layer and direct energy measurement can be applied to their produced γ-rays.

Figure 6 shows a diagram of observed γ-rays plotted with their lateral distance from the energy-weighted center of the interaction r_γ, as the X-axis and their energies as the Y-axis.

Assuming that the average location of the interactions is the producing layer is 120 cm above the lower chambers, the diagram gives directly the P_T-distribution of γ-rays. At the same time, it shows that there is practically no detection loss of γ-rays with

energy $\geqslant$250 GeV produced in C-jets.

Location of the individual C-jet in the producer can be estimated from the $2\gamma - \pi^{o}$ coupling, as our previous analysis on atmospheric interactions. The P_T-distribution of γ-rays can be constructed on this basis, too. Figure 7 gives the two experimental results on the $P_{T\gamma}$-distribution, and they agree with each other as it should be.

Observation of Fire Balls

The observed events are classified into three groups according to their total energy $\sum E_\gamma$, namely those with $\sum E_\gamma$ of 3-6 TeV, 6-12 TeV and higher. We construct for each group the composite distribution of energy E_γ, angle θ_γ of produced γ-rays. All the results are presented in Fig. 8 and 9.

For the lower energy group ($\sum E_\gamma = 3 - 6$ TeV), the angular distribution in Fig. 9 suggests isotropic emission from a single fire ball. Furthermore, comparison of the energy distribution and the P_T-distribution shows that the both are in agreement with the scale change $E_\gamma = \gamma_H P_{T\gamma}$, and value of the parameter is $\gamma_H = 5000$ as seen in Fig. 10. This value agrees well with that obtained by applying the half angle method for the angular distribution*. Thus the conclusion is that almost all of observed γ-rays here are emitted from a fire ball moving with γ-factor $\gamma_H = 5000$ in the laboratory system.

* See Fig. 9.

A similar analysis can be applied to a higher energy group ($\sum E_\gamma$ = 6 - 12 TeV). Assuming a similarity relation for the moment, one takes only γ-rays with $E_\gamma \geq$ 500 GeV since the concerned energy is doubled in an average. A comparison of the distribution of E_γ and P_{T_γ} gives γ_H = 8000 for γ-factor of the fire ball as seen in Fig. 11. This value, γ_H = 8000, is again in good agreement with one obtained from the angular distribution. Thus all the results show again a moving fire ball similar to the lower energy region ($\sum E_\gamma$ = 3 - 6 TeV).

For events of this group, γ-rays of still lower energy are observed down to 200 GeV. If all such low energy γ-rays of 200 - 500 GeV are included in the statistics, the angular distribution shows deviation from an isotropic emission as seen in Fig. 9. This can be interpreted as showing contribution from the second fire ball.

π^o-Mesons from Fire Balls

Characteristics of the fire ball can be explored further by using 2γ-π^o coupling. First a consistency of 2γ-π^o coupling can be checked by constructing the energy disparity parameter ξ, defined by

$$\xi = (E_2 - E_{min}) / \frac{E_1 + E_2}{2} - E_{min} .$$

E_1 and E_2 are energies of a coupled pair, and E_{min} is the detection threshold, 200 GeV. Fig. 12 shows a histogram of the parameter ξ, which appears consistent with the uniform distribution.

Energy and momentum in the fire-ball rest system, E_π^* and P_π^*, are constructed for every identified π^o-mesons applying Lorentz transformation with γ_H estimated above. The result are plotted in the diagram with parallel component of the momentum $P_{//\pi}^*$ as X-axis and its transverse component $P_{T\pi}^*$ as y-axis, as shown in Fig. 13. One sees existence of a few π^o-mesons moving backward with large momenta, which apparently belong to the second fire ball. After taking out those, the distribution is found consistent with isotropic emission of π^o-mesons.

The momentum distribution in the fire-ball rest system, $f(P_\pi^*)\, dP_\pi^*$, are now constructed. As seen in Fig.14, the experimental results are well represented by the following formula,

$$f(P_\pi^*)\, dP_\pi^* = \exp(-P^*/Po^*)\; p^*\, dp^*$$

with

$$Po^* = 175 \pm 25 \text{ MeV} .$$

Summation of energies of π^o-mesons from a fire ball, $\sum_{f.b.} E_\pi^*$, gives information on mass of a fire ball. Fig. 15 presents a histogram of $\sum_{f.b.} E_\pi^*$, and the average value is,

$$\langle \sum_{f.b.} E_\pi^* \rangle \; 1.0 \pm 0.2 \text{ GeV}$$

Comparison with Balloon E.C.C. Experiment

The balloon experiment of Japanese Emulsion Group in 1956 gives extensive data of nuclear interactions in lower energy regions. The same analysis on the fire ball is applied to the

data of the 9 observed nuclear events with energies $\sum E_\gamma = 300\text{-}700$ GeV. The detection threshold there is as low as 20 GeV because of low background, so that quality of the data are more or less the same as in the present experiment.

Fig. 16 presents the results on the distribution on the energy E_π, transverse momentum $P_{T\pi}$, and the emission angle θ_π of π^o-mesons. They indicates existence of a fire ball of the Lorentz transformation factor $\gamma_H = 670$, and characteristics of a fire ball have no detectable difference compared to the higher energy case.

H-quantum Theory

Hasegawa proposed in 1961 existence of energy quantum in fire balls produced by the extremely high energy nuclear interactions. He found that mass of this quantum (called H-quantum) is about 2 - 3 times nucleon mass and magnitude of 4-momentum transfer in H-quantum production is of the same order of magnitude of H-quantum mass. [4]

The present experiment provided evidence for existence of H-quantum in nuclear interactions covering a wide range of energies, $\sum E_\gamma$ = 300 GeV - 10.000 GeV

PART III - ATMOSPHERIC INTERACTIONS

Atmospheric Interactions of Higher Energy

For interactions of still higher energy, $\sum E_\gamma \geq 10$ TeV, we have for the moment only informations from the atmospheric interactions. In order to avoid ambiguities in interpretation caused by possible atmospheric cascade processes and secondary interactions, we imposed a severe selection criterion on the estimated production height as $50\ m < h < 1000\ m$.

Table II gives number of thus selected events for the present analysis.

Change of $P_{T\gamma}$ with Interaction Energy

In order to see possible change of mass of a fire ball as one goes into higher energy region, one constructs summation of P_T of γ-rays for all events including C-jets as well as atmospheric interactions. The summation covers on γ-rays with energy $E_\gamma \geq \frac{1}{10} E_{\pi^0}^{(max)}$, where $E_{\pi^0}^{(max)}$ is the highest energy of π^0-meson in the event.[5] Thus $\sum P_{T\gamma}$ gives a measure of mass of a fire ball.

Fig. 17 shows diagram of $\sum P_{T\gamma}$ and $\sum E\gamma$ for all events. One sees that magnitude of $\sum P_{T\gamma}$ stays nearly constant, $\langle \sum P_{T\gamma} \rangle$ 800 MeV, up to the region of $\sum E_\gamma \sim 20$ TeV. In higher energy region, $\sum E_\gamma > 20$ TeV, onde finds a number of events having $\sum P_{T\gamma}$ of 3 - 4 GeV. This suggests that H-quantum theory holds up to $\sum E_\gamma \sim 20$ TeV and beyond this energy region there appears a heavier

fire ball of mass about five times larger than that of H-quantum.

Fire Ball Analysis

The fire ball analysis in Part II is now applied to the atmospheric interactions. The Atmospheric interactions are divided into four groups, $\sum E_\gamma$ being 10 - 20 TeV, 20 - 50 TeV, 50 - - 100 TeV, and $\geq$ 100 TeV. The composite angular distribution for the four groups are shown in Fig. 18. All of them are found consistent with the isotropic emission from a fire ball.

Result of the analysis on the lowest energy group ($\sum E_\gamma$ = 10 - - 20 TeV) are in good agreement with the previous results on C- -jets, as is seen in figures in Part II. Thus H-quantum is seen up to $\sum E_\gamma$ = 20 TeV.

Characteristics of fire balls are found to change appreciably beyond this energy region. Fig. 19 presents the Lorentz factor γ_H of fire ball in the laboratory system, estimated in various energy region.

One sees that beyond 20 TeV, γ_H does not increase with $\sum E_\gamma$. This shows that energy increase does not go into the translation motion but rest energy of a fire ball.

Fig. 20 presents summation of energies of π^o-mesons from a fire ball, $\sum_{f.b.} E^*_\pi$. When the interaction energy is around 100 TeV, $\sum_{f.b.} E^*_\pi$ is about 5 GeV. Mass of a fire ball there must be about 5 times of that of H-quantum, 10 - 15 GeV.

SH-Quantum Hypothesis

Authors propose a new hypothesis of super heavy quantum (SH-quantum) appearing in nuclear interactions beyond $\sum E_\gamma \sim 50$ TeV. Considering that H-quantum is closely connected with inner structure of a meson, we suggest that SH-quantum could be intimately connected with inner structure of a baryon. Future experiment will give us an answer to the SH-quantum problem.

Some Characteristics of SH-Quantum

A possible decay scheme of the SH-quantum is suggested as,

SH-quantum --- H-quantum --- π-mesons .

Assuming that the both decay are isotropic, one can work P_T-distribution of π-mesons measured from axis of motion of SH-quantum.

Fig. 21 gives comparison of experimental and calculated P_T-distribution. Calculation is made assuming Planck distribution of π^o-meson in H-quantum and isotropic decay of SH-quantum into H-quantum with γ-factor γ_{H^*}. If one constructs the distribution from the events with $\sum P_{T\gamma} \geq 2$ GeV, selecting possible SH-quantum events, onde finds that the distribution has long tail in agreement with the above decay scheme with $\gamma_H^* = 2.0$.

Special Event

In this chamber, a clean event with extremely high energy was observed. The schematic view is shown in Fig. 22. Four generations of interactions are observed in this event. The height of

the primary act is estimated as about 3km above the chamber, the second at 200 m, the third at the producing layer, and the last in the lower chamber. Since the whole event has rather complex feature, only main parts of the event, the secondary act (II), are shown in Fig. 23 a and b.

The interaction height of the secondary act was determined directly as shown in Fig. 24. Two of secondary particles from this interaction made pb-jets in the upper chamber. One has its origin at 8 c.u. in the upper chamber with energy of $\Sigma E_\gamma = 37$ TeV and the other has its origin at 12 c.u. with energy of $\Sigma E_\gamma = 3$ TeV. The tails of these pb-jets are observed in the lower chamber. Since fortunately 3 TeV pb-jet experienced only a few cascade length to penetrate down to the lower chamber, the direction of shower axis is disturbed only slightly by multiple scattering of shower particles [6]. Measuring the distances between these two shower axes at the upper chamber and the lower chamber respectively, r_1 and r_2 in Fig. 24, the interaction height of the secondary act is estimated directly as 160 m $\pm$ 30 m. Another way to estimate the height is the method of coupling of 2γs to π_0 mesons. The obtained results are consistent with each other.

Since the primary act occurred at rather high altitude and the secondary act has its origin quite near above the chamber, the secondaries of each events are observed separatly. Furthermore, because the γ-rays in the secondary act can reach the chamber without suffering cascade proccess, the analysis can be made with

out ambiguity.

The features of nuclear particles and π_o mesons produced in this interaction are shown in Fig. 25 in the form of correlation between the energy and the emission angle in the laboratory system.

* * *

TABLE I - LIST OF EXPOSURES

	Area (m^2)	Area × Time (m^2 year)	Total thickness (cm Pb)
Norikura			
1959	3.0	1.2	4
1960 - I	7.2	6.0	4
1960 - II	1.6	0.2	10
1961	5.4	2.7	5
1962 - I	14.0	14.6	6
1962 - II	8.8	16.9	13
1964 (producer)	3.0	2.5	22
1965	2.0	2.0	37
Total	45.0	46.1	
Chacaltaya			
1962 - I	0.4	0.05	6
1962 - II	1.2	0.3	6
1962 - III	6.0	1.2	6
1963	5.6	2.8	10
1964	6.0	5.25	29
1965 (producer)	6.0	5.25	28
Total	25.2	14.95	

TABLE 1 - LIST OF EXPOSURES

	Area (m^2)	Area × Time (m^2 year)	Total Thickness (cm Pb)
Norikura			
1952 I	2.0	0.8	4
1952 II (Producer)	1.0	0.4	11
1960 - I	7.2	6.0	4
1960 - II	1.6	0.2	10
1961	5.4	2.7	5
1962 - I	14.0	14.6	6
1962 - II	8.8	16.9	13
1964 (Producer)	3.0	2.5	22
1965	2.0	2.0	37
Total	45.0	46.1	
Chacaltaya			
1962 - I	0.4	0.05	6
1962 - II	1.2	0.3	6
1962 - III	6.0	1.2	6
1963	5.6	2.8	10
1964	6.0	5.25	29
1965 (Producer)	6.0	5.25	28
Total	25.2	14.95	

TABLE II - NUMBER OF JETS ANALYSED

	Energy Interval	No. of Jets	Lorentz factor of fire ball
C-Jets	0.3 - 0.7 TeV	9	670
	3 - 6	10	5000
	6 - 12	7	8000
Atmospheric Jets	10 - 20	10	15000
	20 - 50	11	22000
	50 - 100	4	18000
	100 -	3	

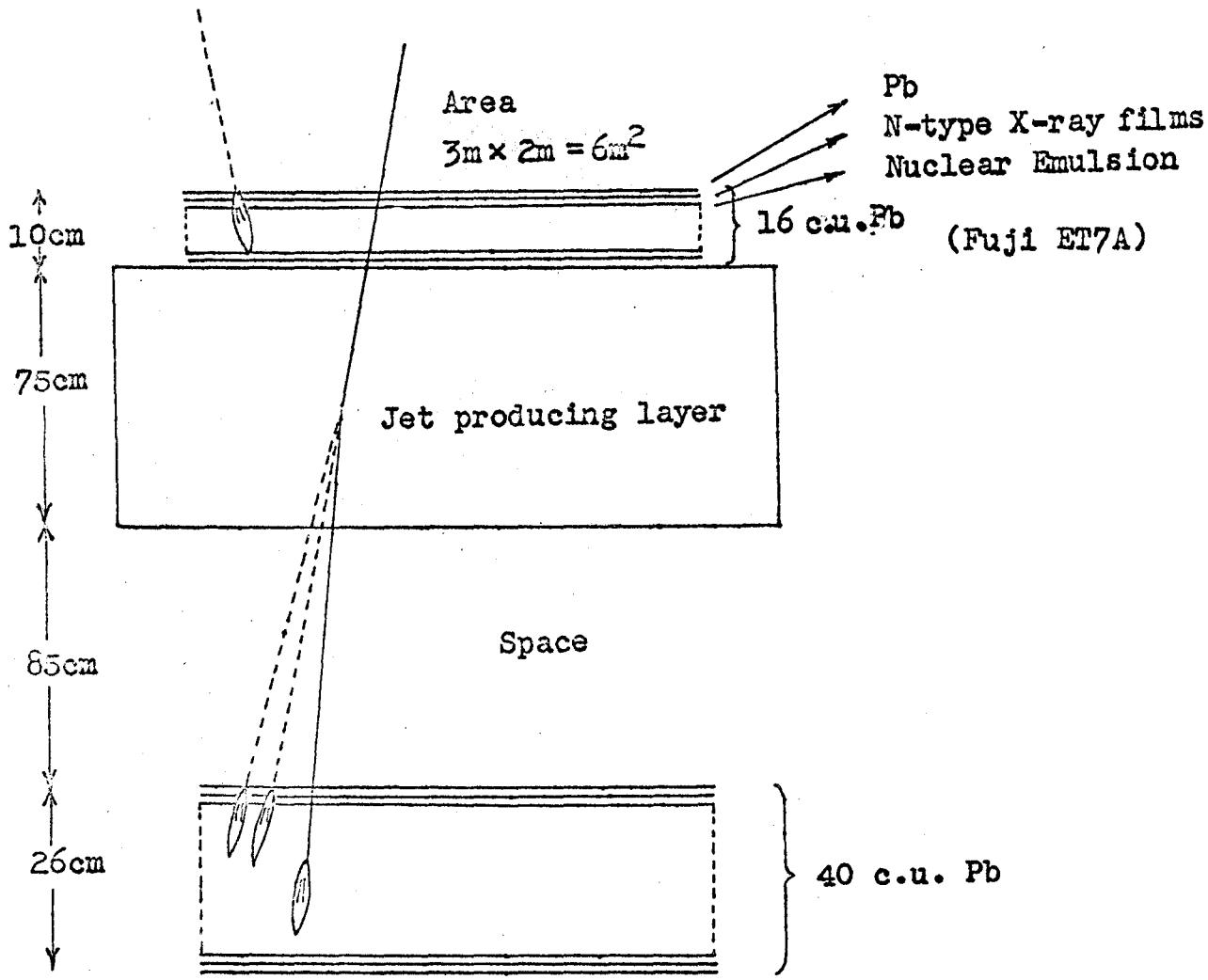

Fig. 1 - Design of the Chamber

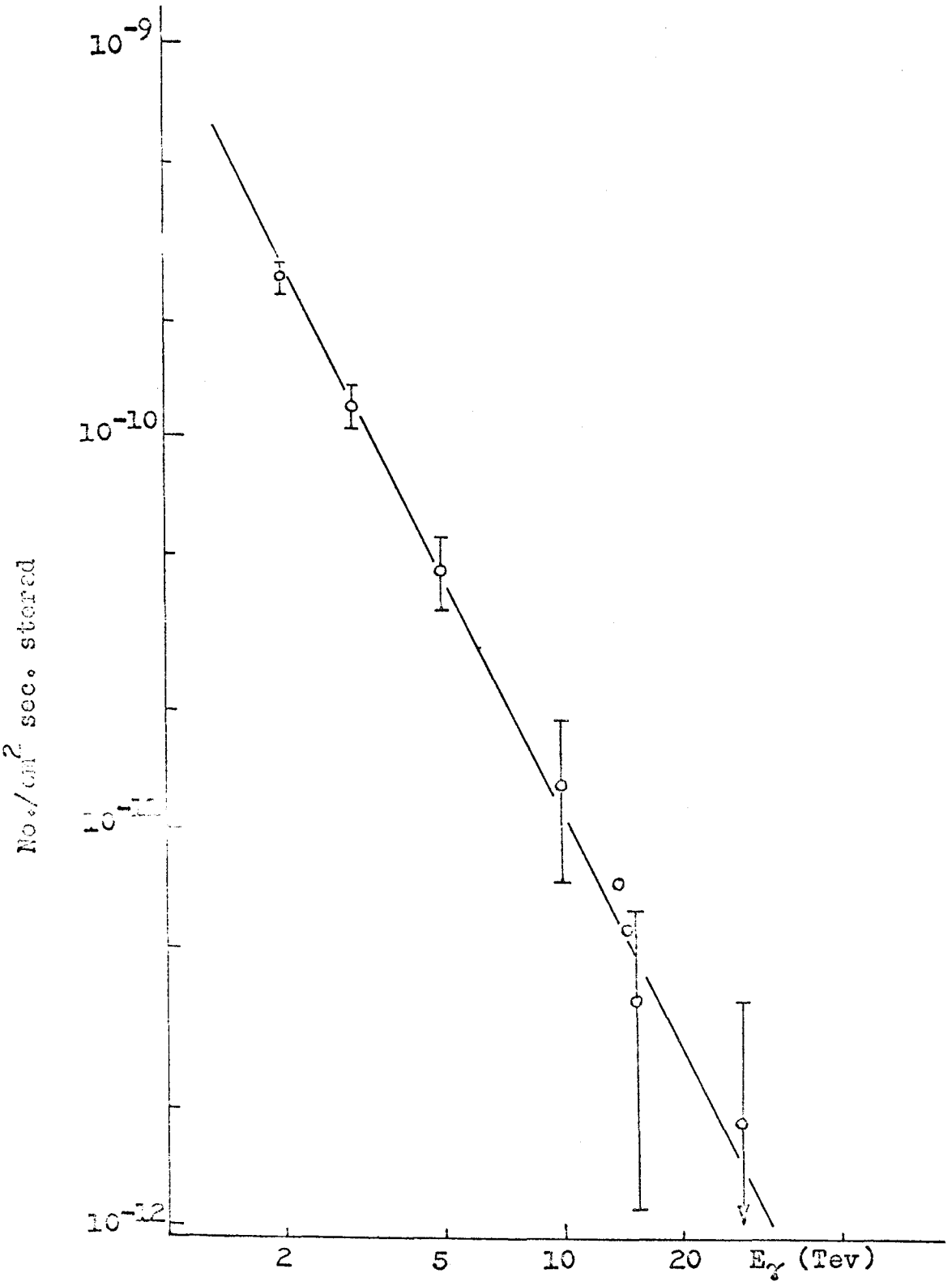

Fig. 2 - Energy Spectrum of $S_2\gamma$

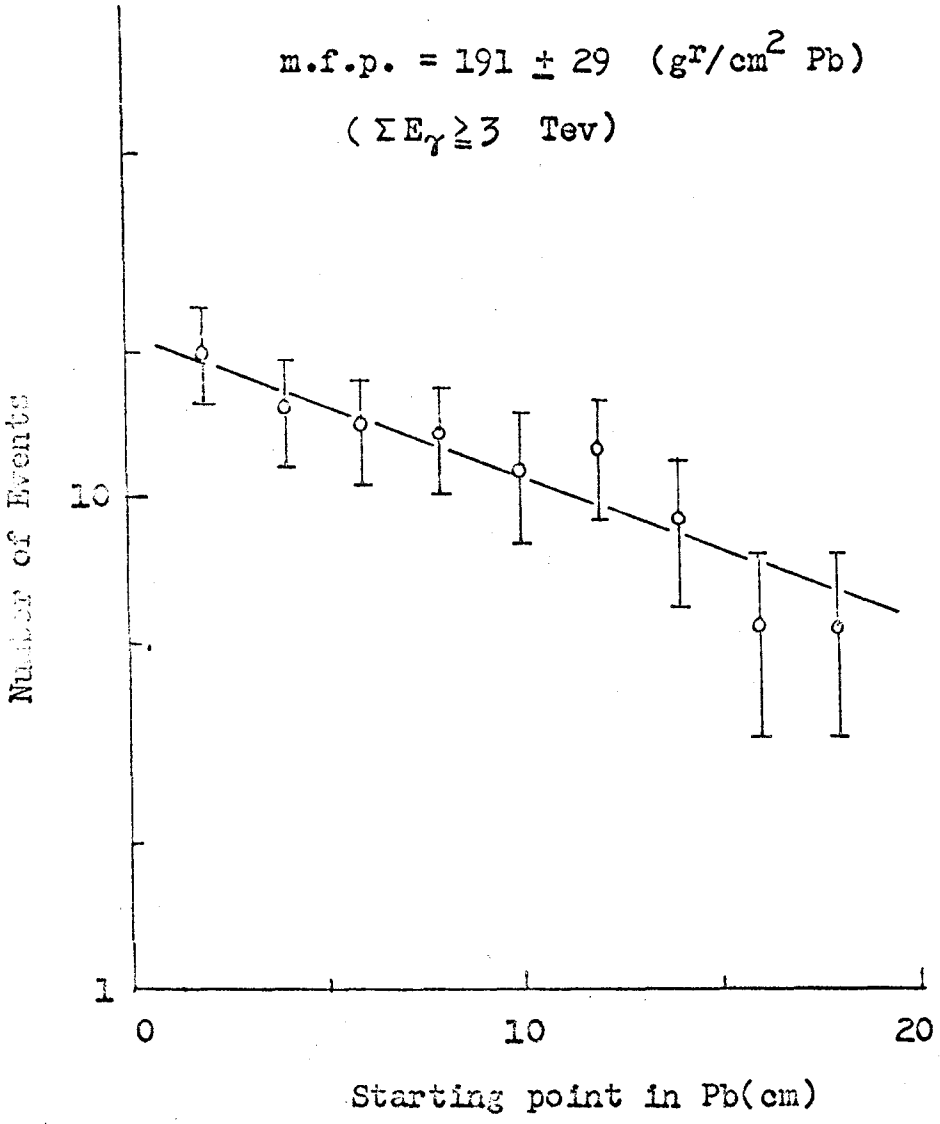

Fig. 3 - Interaction mean free path of nuclear active particles

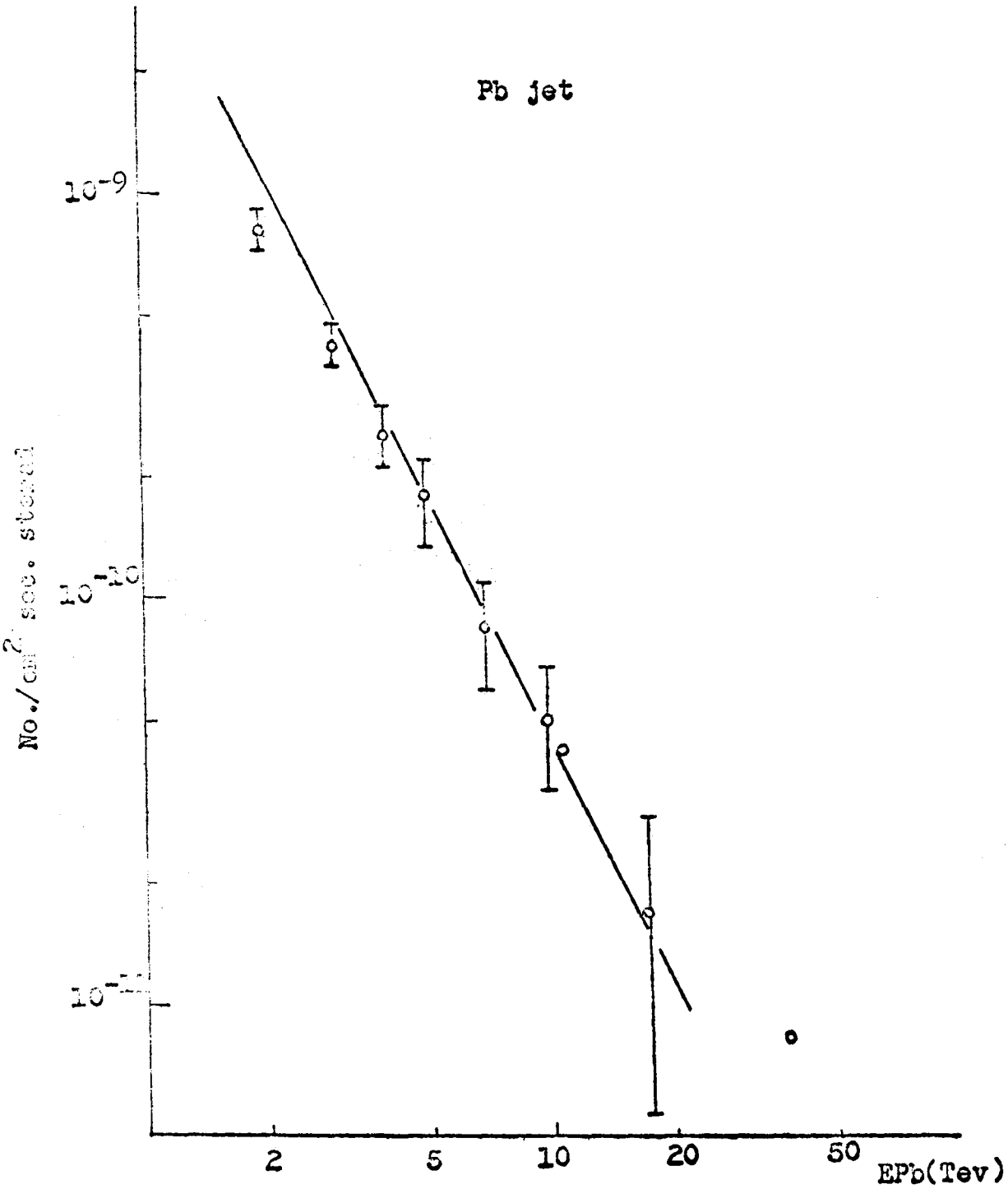

Fig. 4 - Energy spectrum of Pb-jet

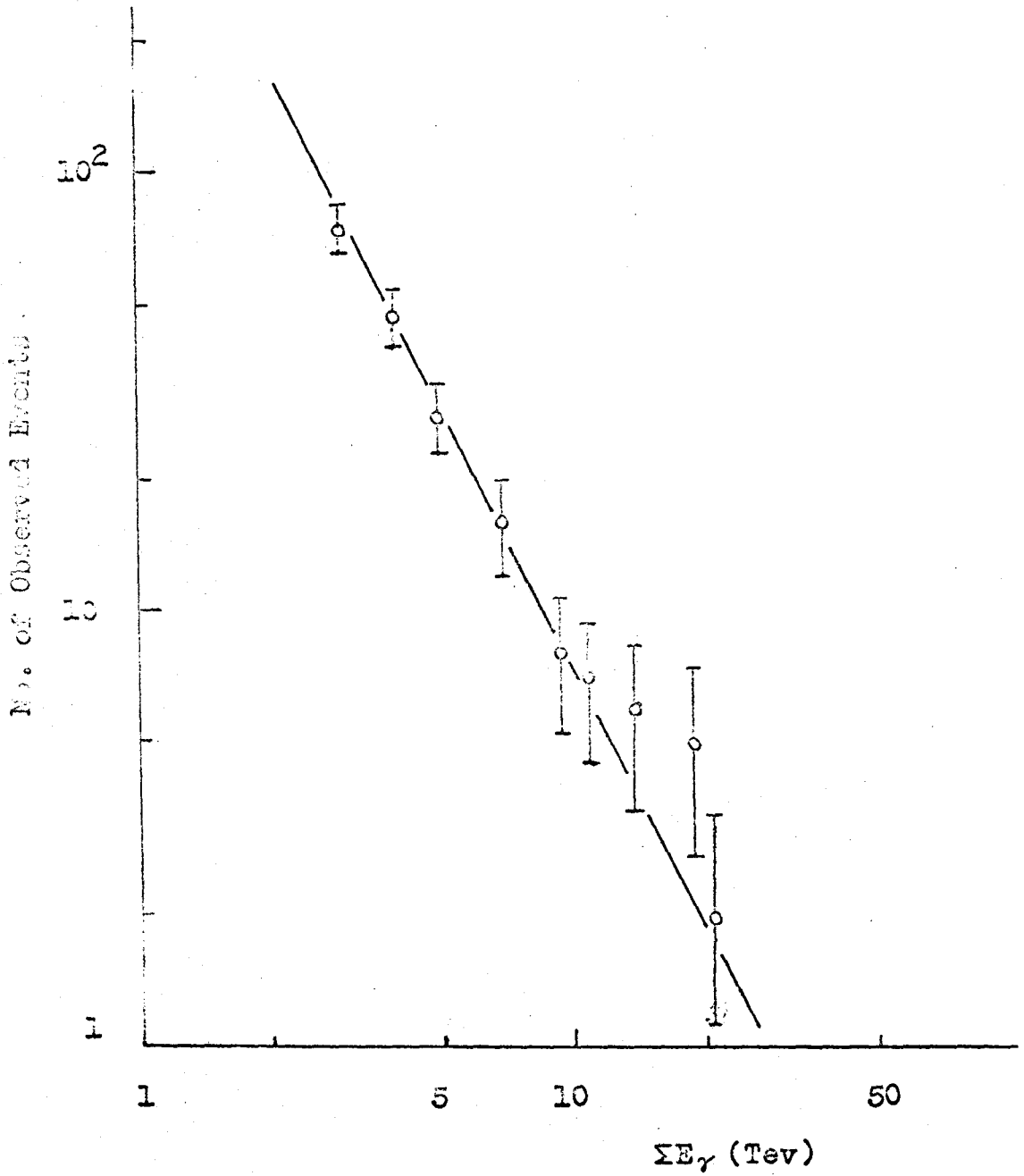

Energy Spectrum of C-jet

Fig. 5

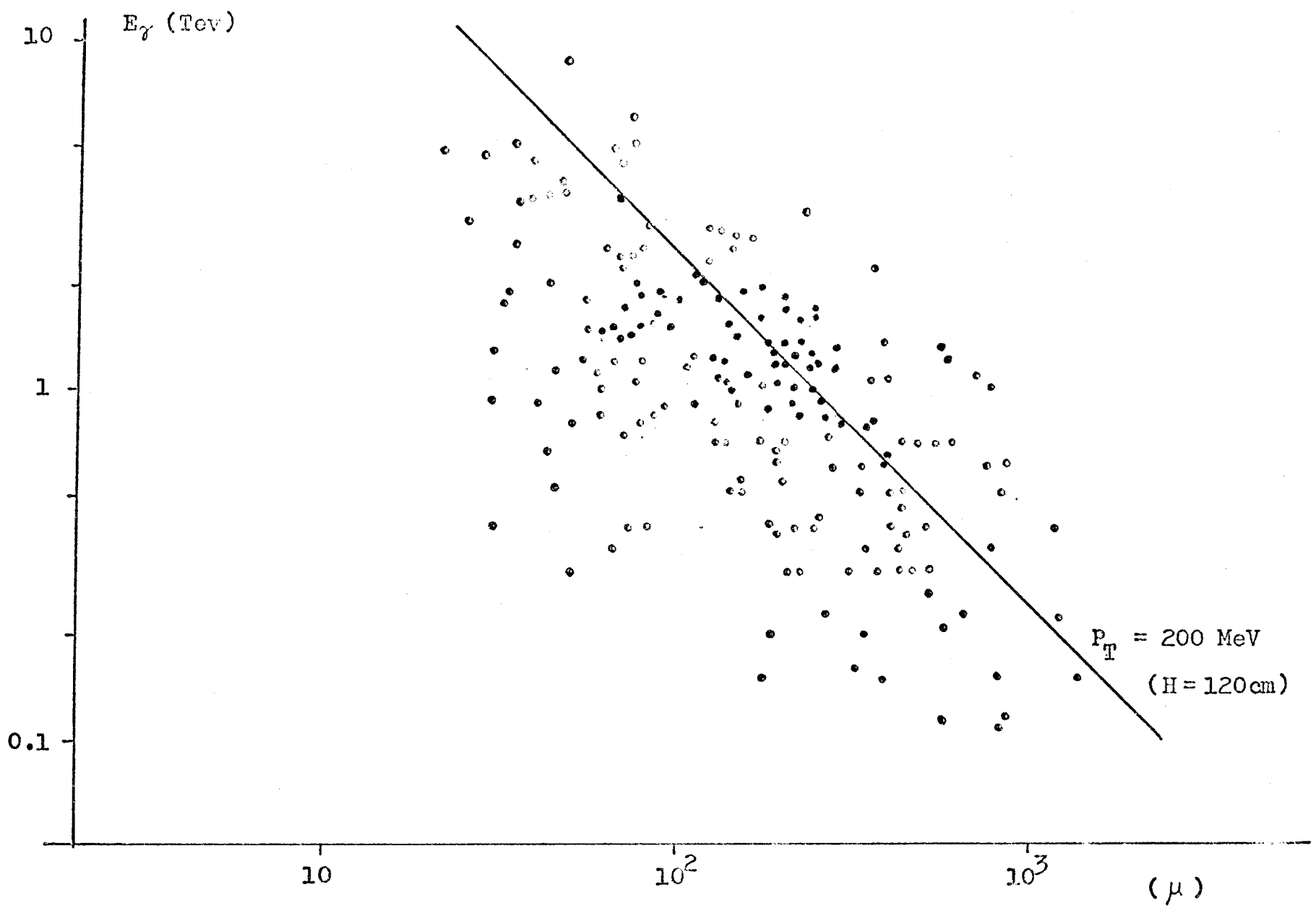

Lateral Distance
Fig. 6

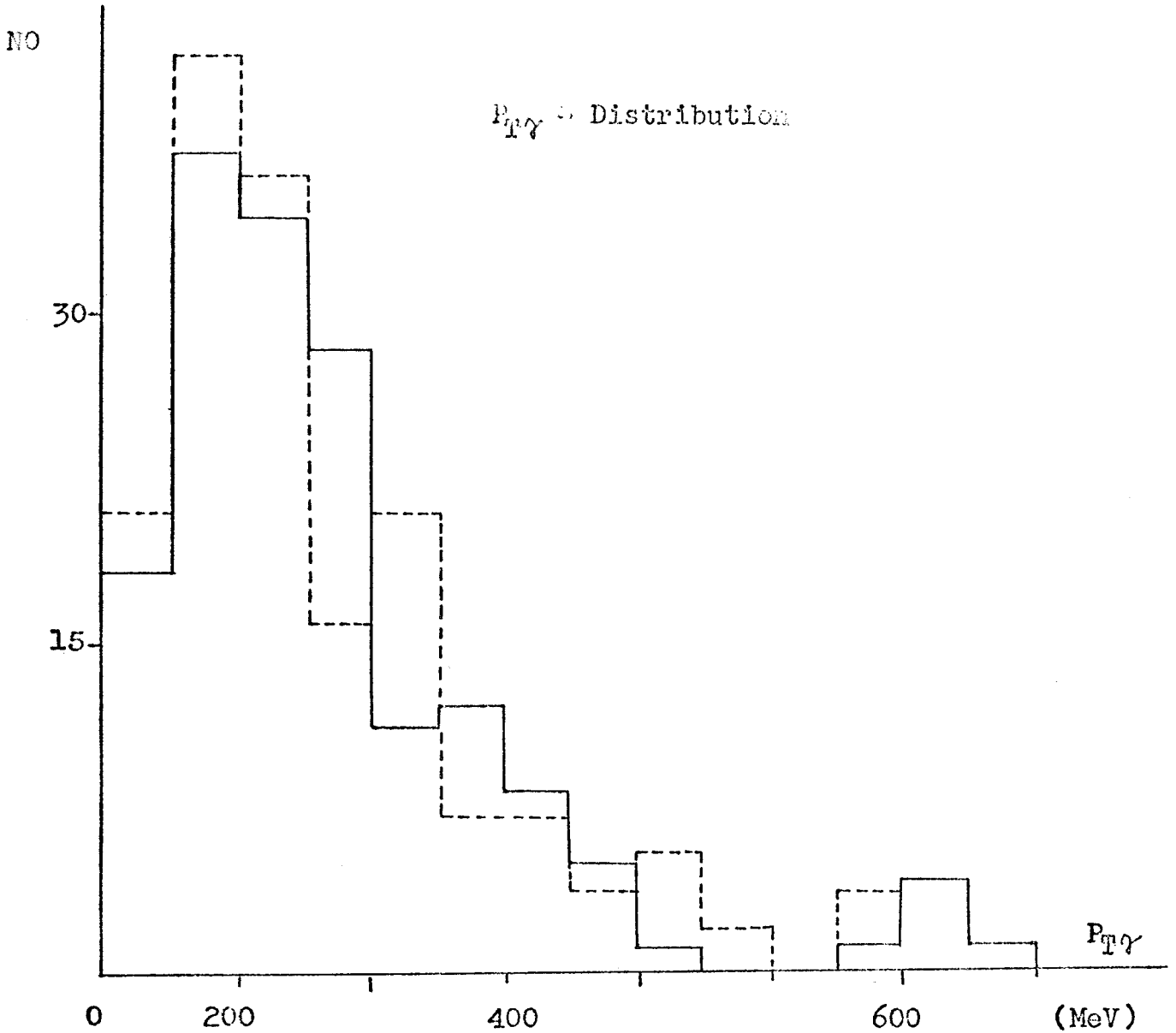

Fig. 7

ANGULAR DISTRIBUTION

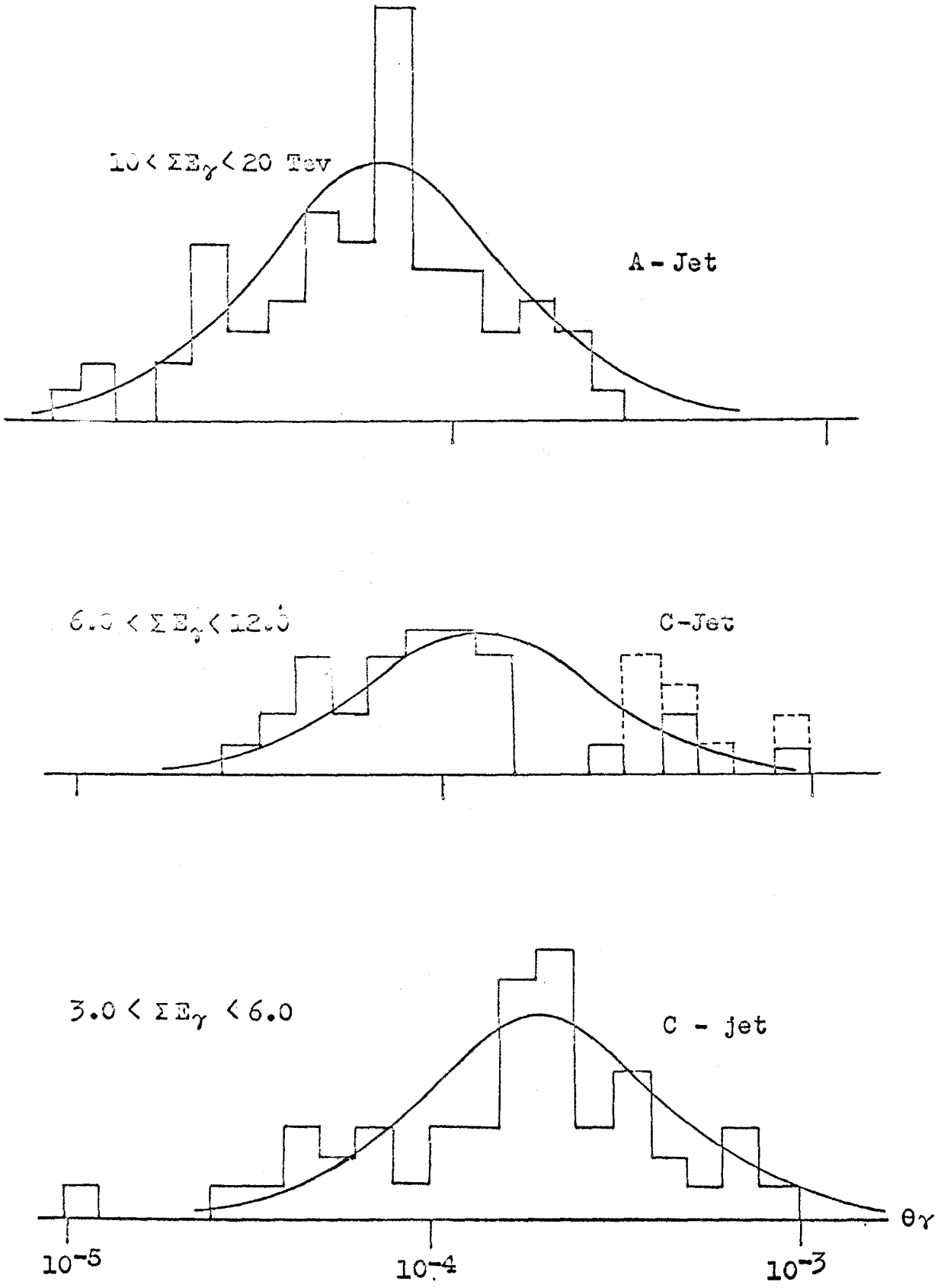

Fig. 8

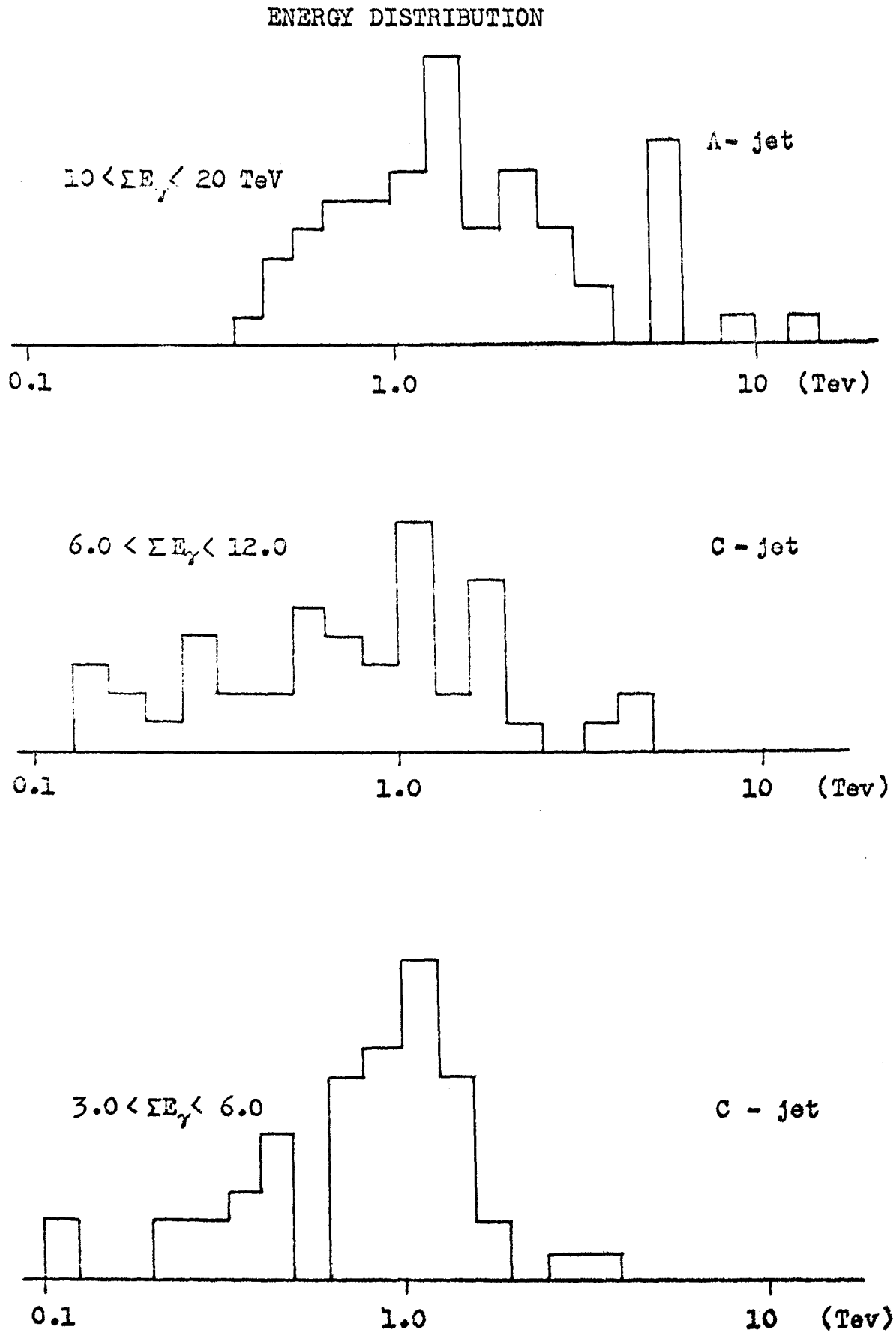
ENERGY DISTRIBUTION
10 < ΣE_γ < 20 TeV
A - jet
0.1
1.0
10 (Tev)
6.0 < ΣE_γ < 12.0
C - jet
0.1
1.0
10 (Tev)
3.0 < ΣE_γ < 6.0
C - jet
0.1
1.0
10 (Tev)

Fig. 9

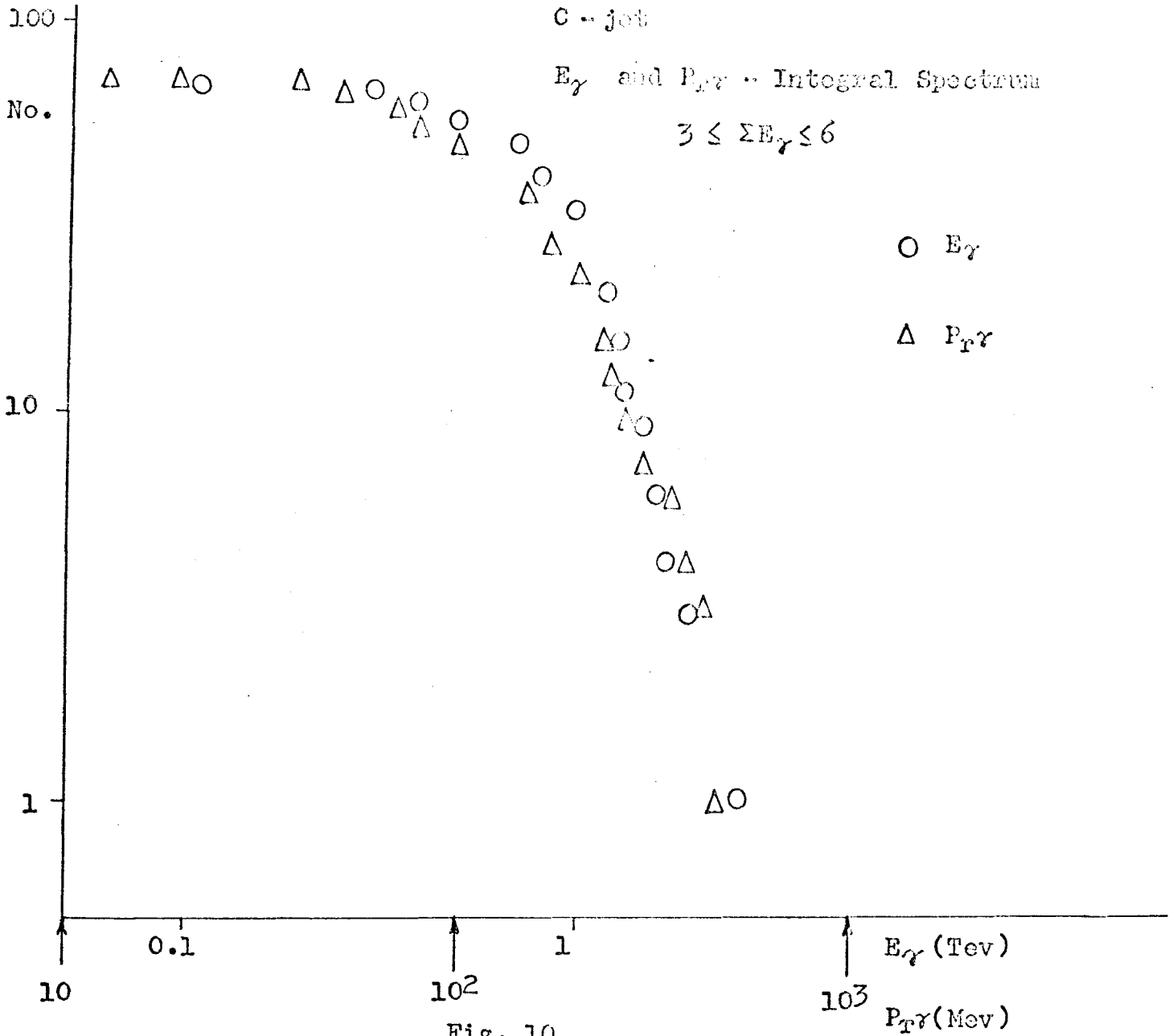
C - jet
E_γ and $P_T\gamma$ - Integral Spectrum
$3 \leq \Sigma E_\gamma \leq 6$
100
No.
10
1
○ E_γ
△ $P_T\gamma$
0.1
1
10
10^2
10^3
E_γ (Tev)
$P_T\gamma$ (Mev)

Fig. 10

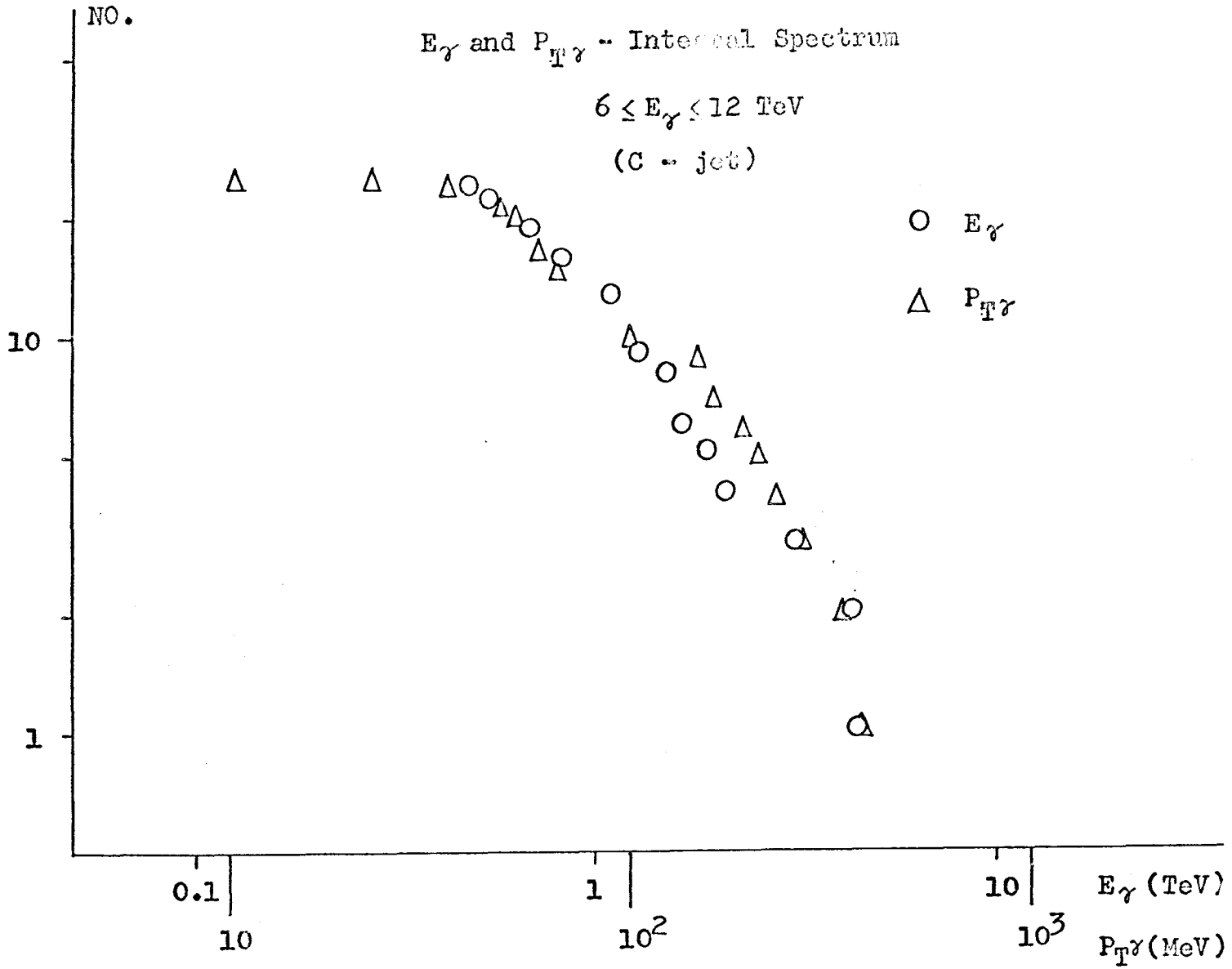
NO.
E_γ and $P_{T\gamma}$ - Integral Spectrum
$6 \leq E_\gamma \leq 12$ TeV
(C - jet)
E_γ
$P_{T\gamma}$
10
1
0.1
1
10
E_γ (TeV)
10
10^2
10^3
$P_{T\gamma}$ (MeV)

Fig. 11

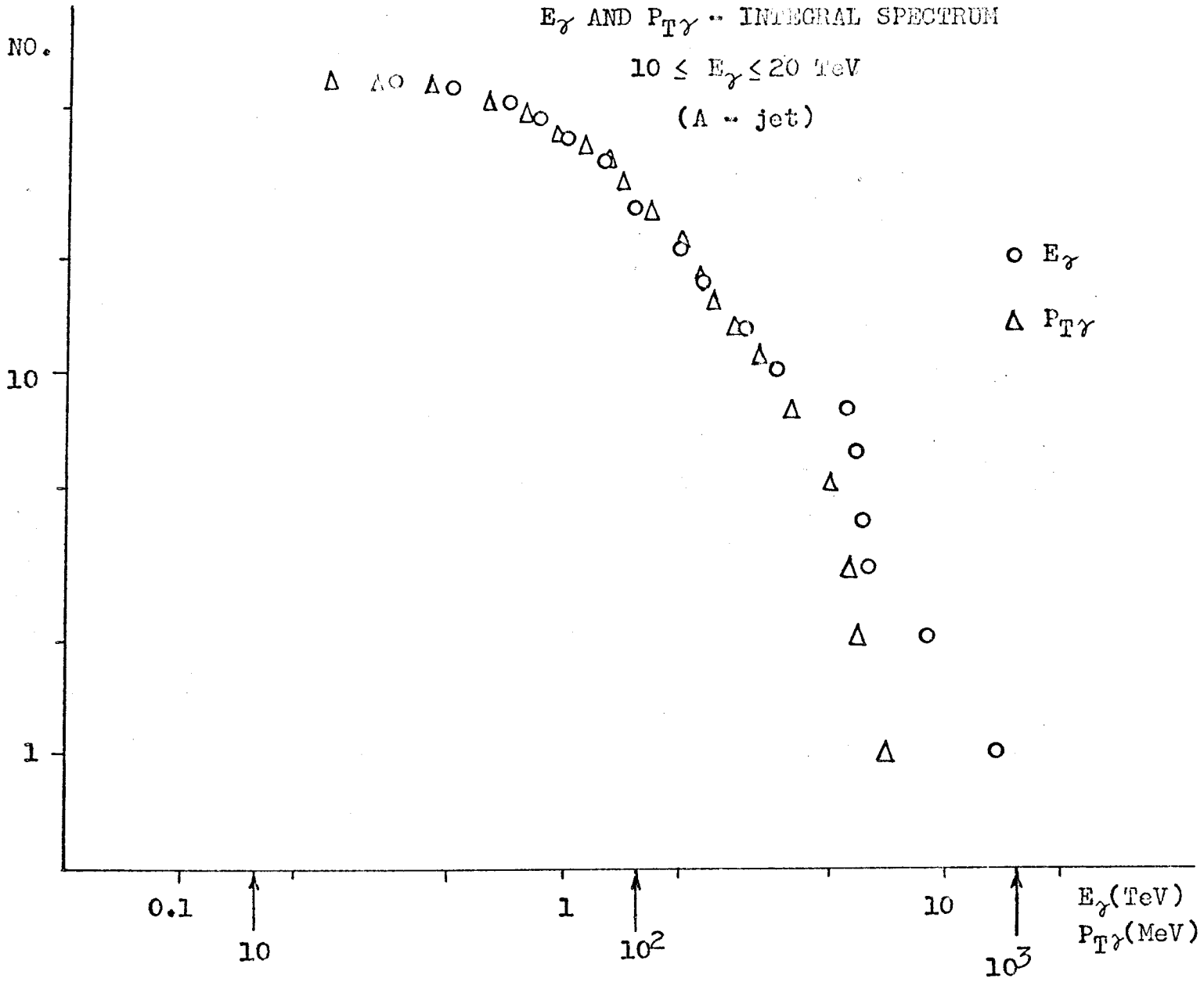
E_γ AND $P_{T\gamma}$ -- INTEGRAL SPECTRUM
$10 \leq E_\gamma \leq 20$ TeV
(A -- jet)
NO.
10
1
E_γ
$P_{T\gamma}$
0.1
1
10
10
10^2
10^3
E_γ(TeV)
$P_{T\gamma}$(MeV)

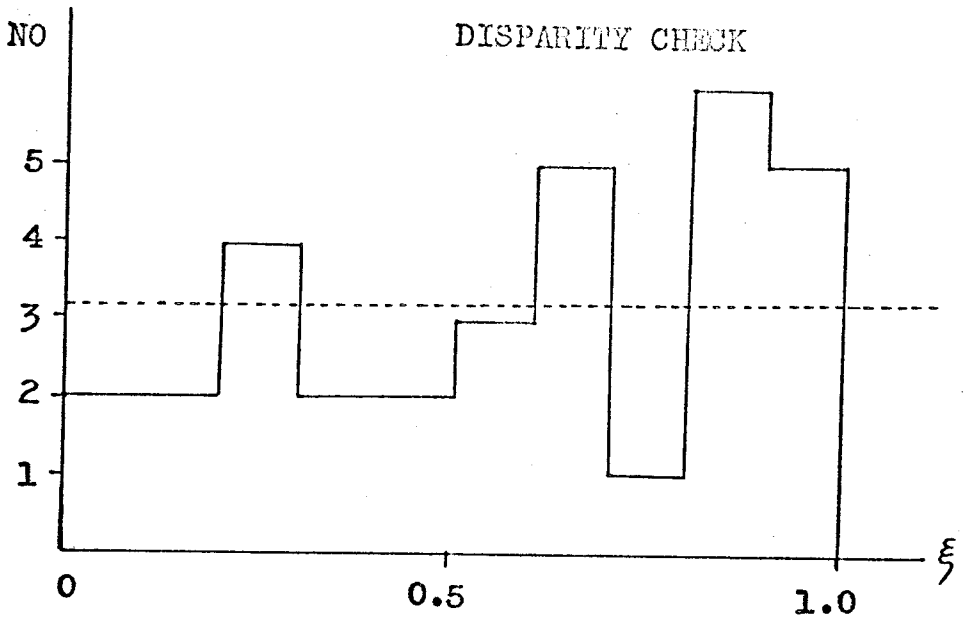

Fig. 12

Fig. 13

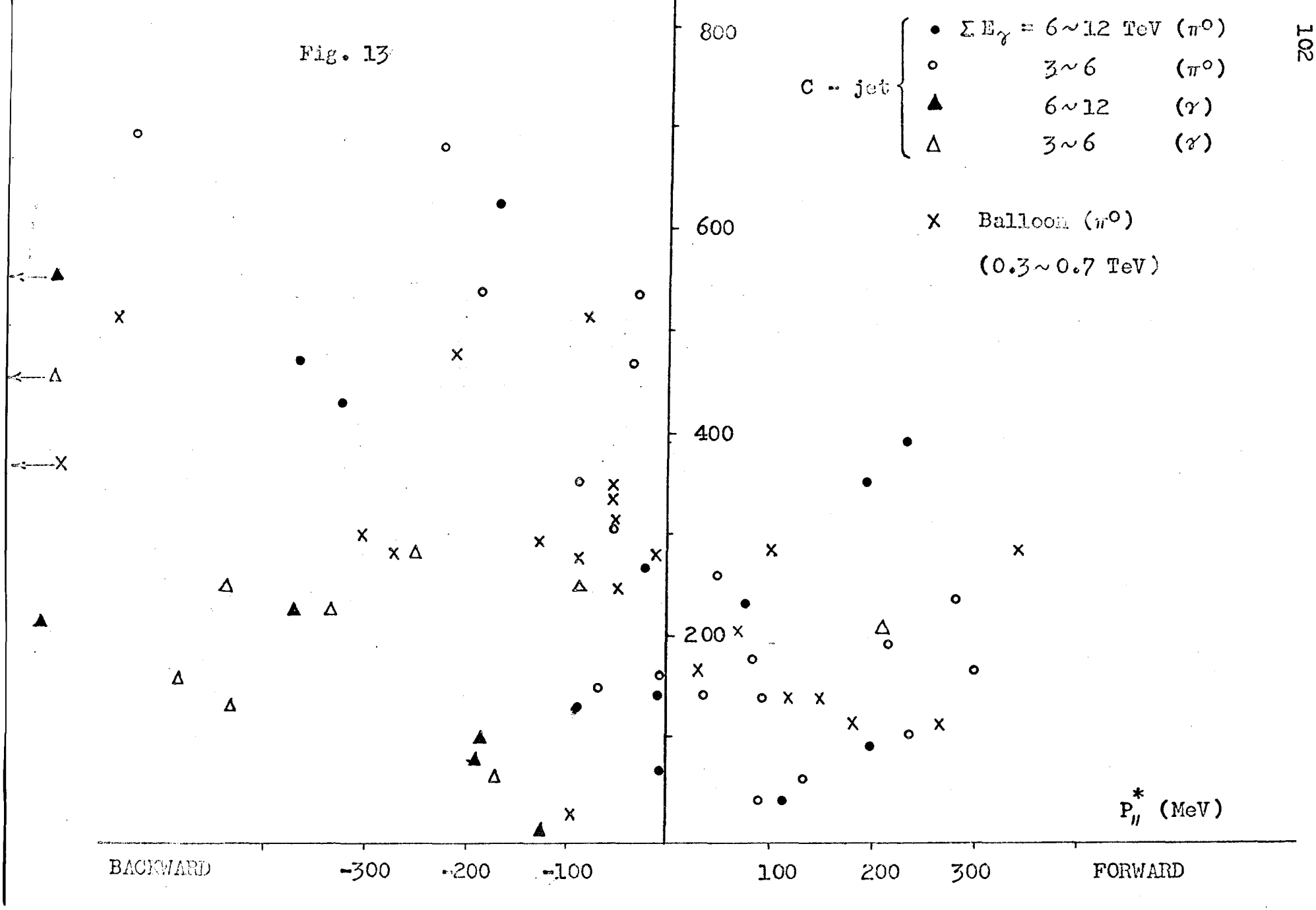
C - jet
• ΣE_γ = 6~12 TeV (π^0)
○ 3~6 (π^0)
▲ 6~12 (γ)
△ 3~6 (γ)
× Balloon (π^0)
(0.3~0.7 TeV)
800
600
400
200
BACKWARD
-300
-200
-100
100
200
300
FORWARD
$P_{//}^*$ (MeV)

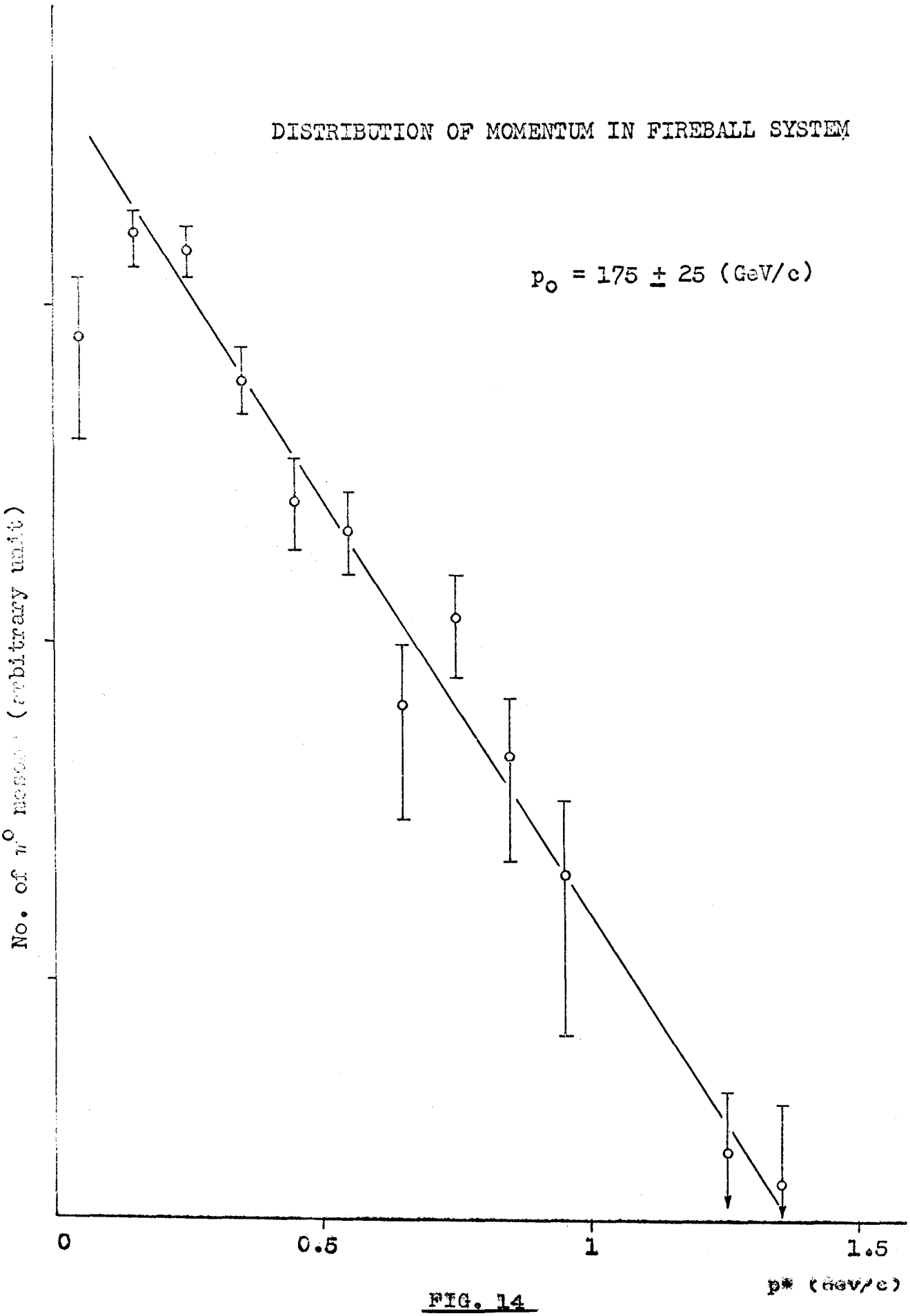
DISTRIBUTION OF MOMENTUM IN FIREBALL SYSTEM
p_o = 175 ± 25 (GeV/c)
No. of π^o meson (arbitrary unit)
0
0.5
1
1.5
p* (Gev/c)

FIG. 14

FIG. 15 FIRE BALL MASS [illegible]

<MASS> = 1.0 ± 0.2 (GeV)

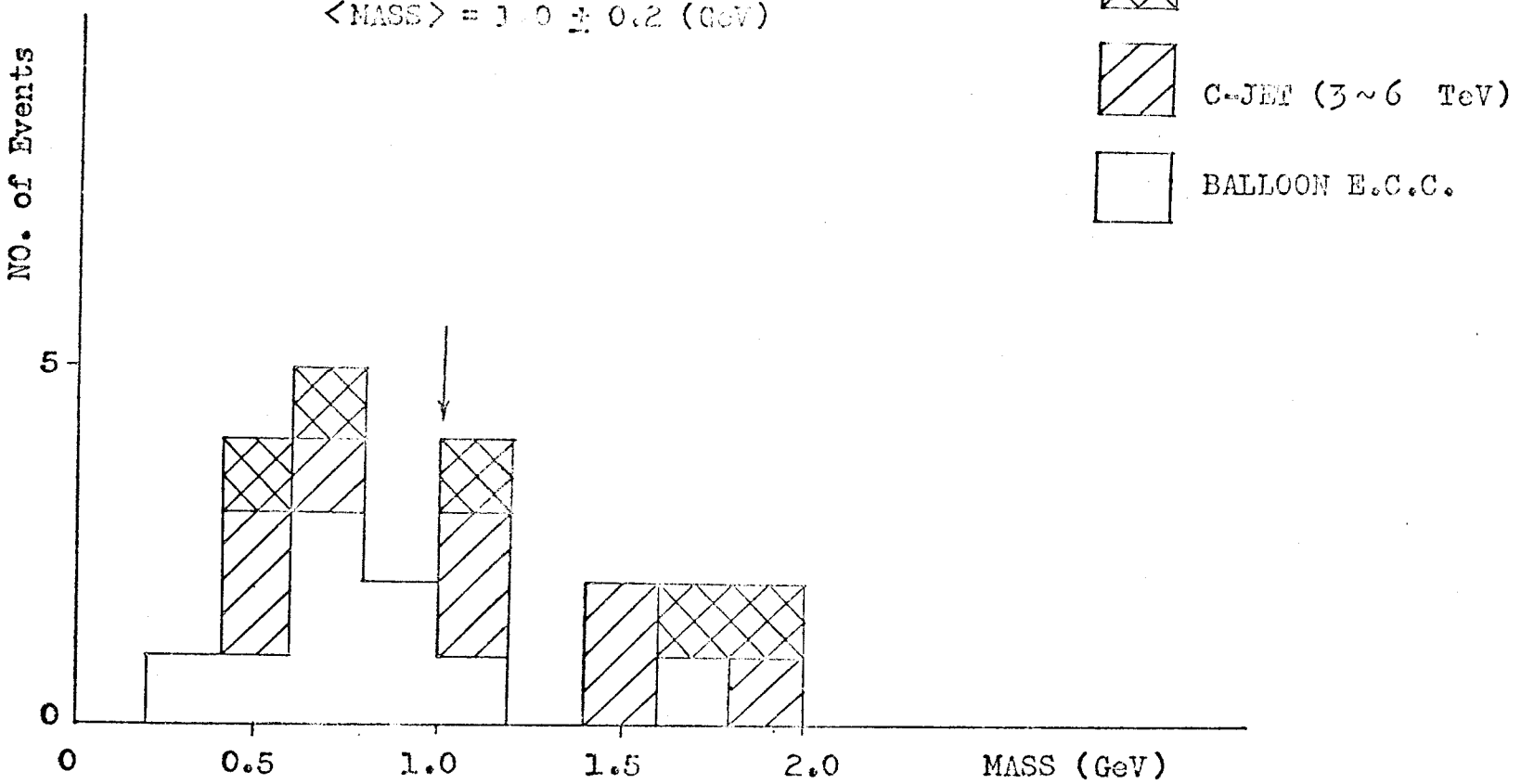

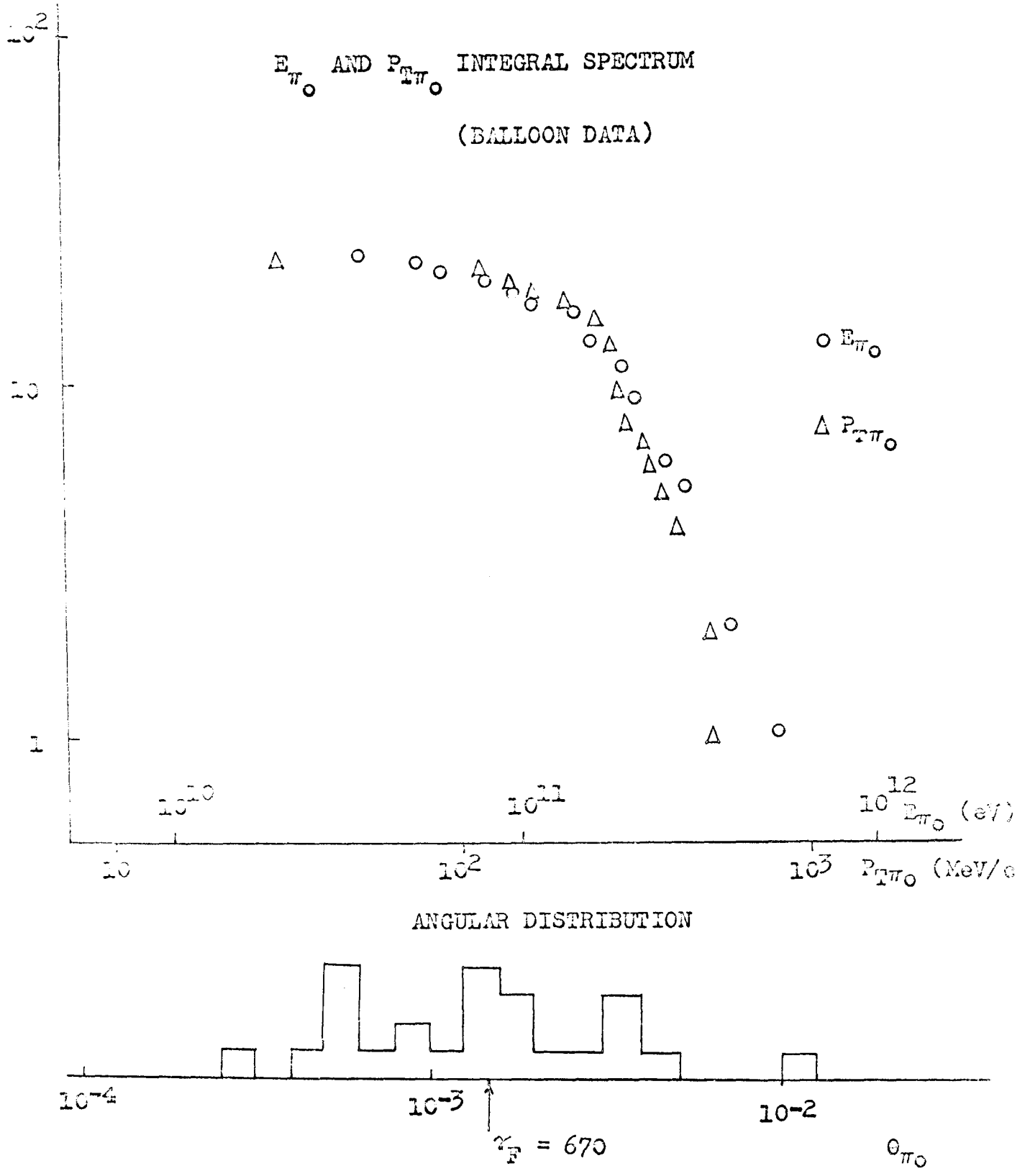
E_{π_o} AND $P_{T\pi_o}$ INTEGRAL SPECTRUM
(BALLOON DATA)
10^2
10
1
E_{π_o}
$P_{T\pi_o}$
10^{10}
10^{11}
10^{12}
E_{π_o} (eV)
10
10^2
10^3
$P_{T\pi_o}$ (MeV/c
ANGULAR DISTRIBUTION
10^{-4}
10^{-3}
10^{-2}
$\gamma_F = 670$
θ_{π_o}

FIG. 16

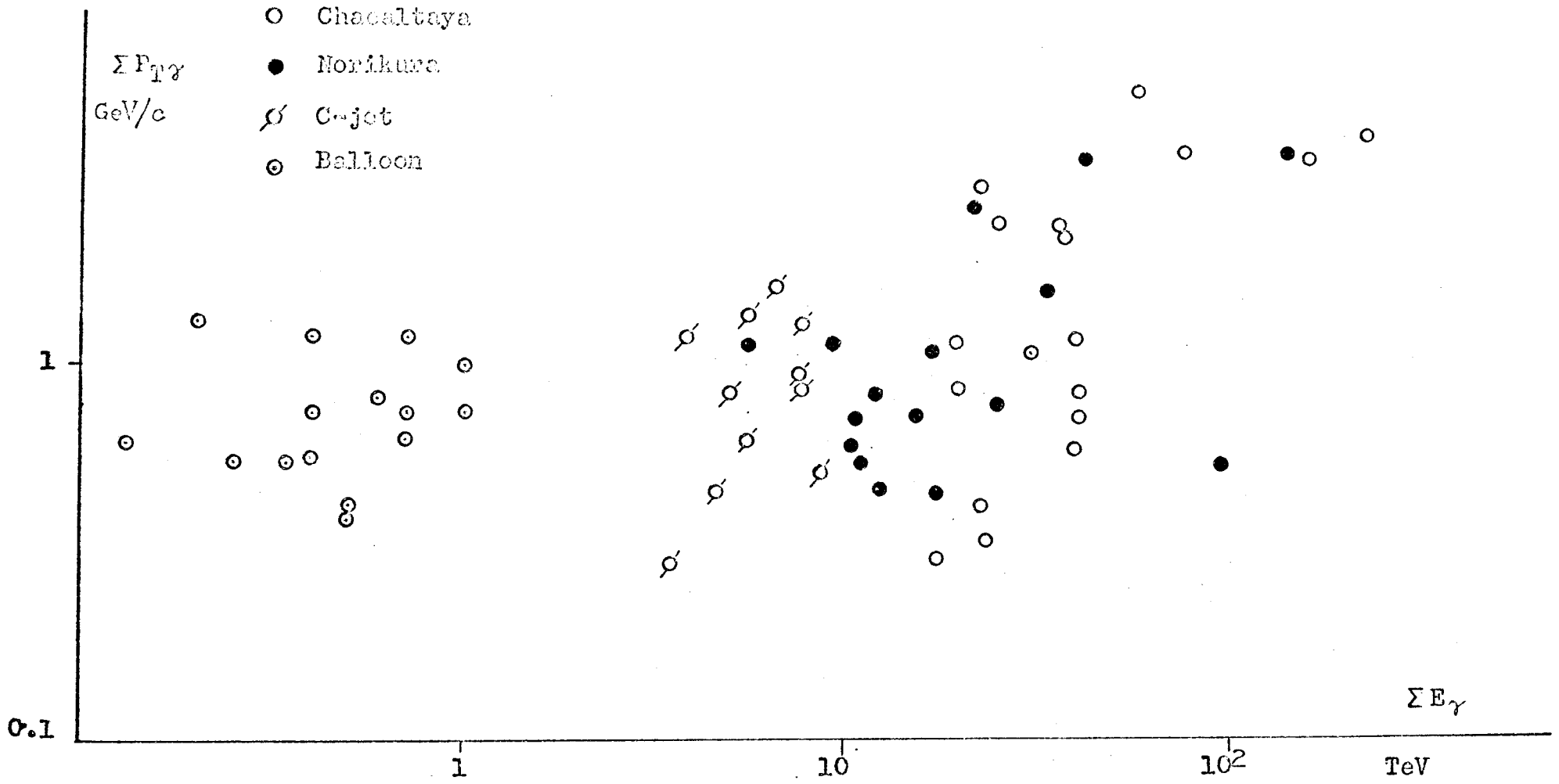
Chacaltaya
Norikura
C-jet
Balloon
$\Sigma P_{T\gamma}$
GeV/c
1
0.1
1
10
10^2
TeV
ΣE_γ

FIG. 17

ANGULAR DISTRIBUTION (AIR INT)

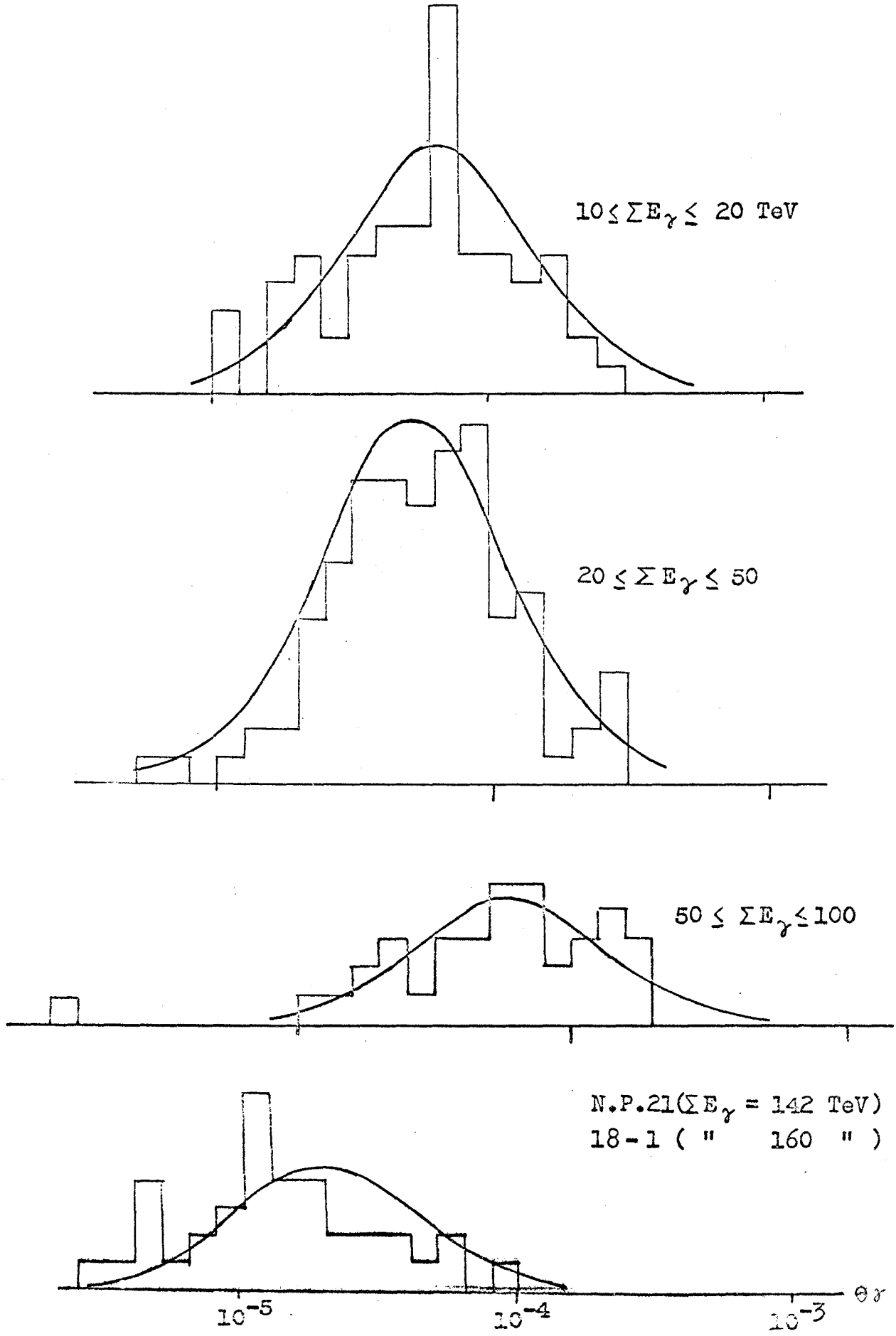

FIG. 19

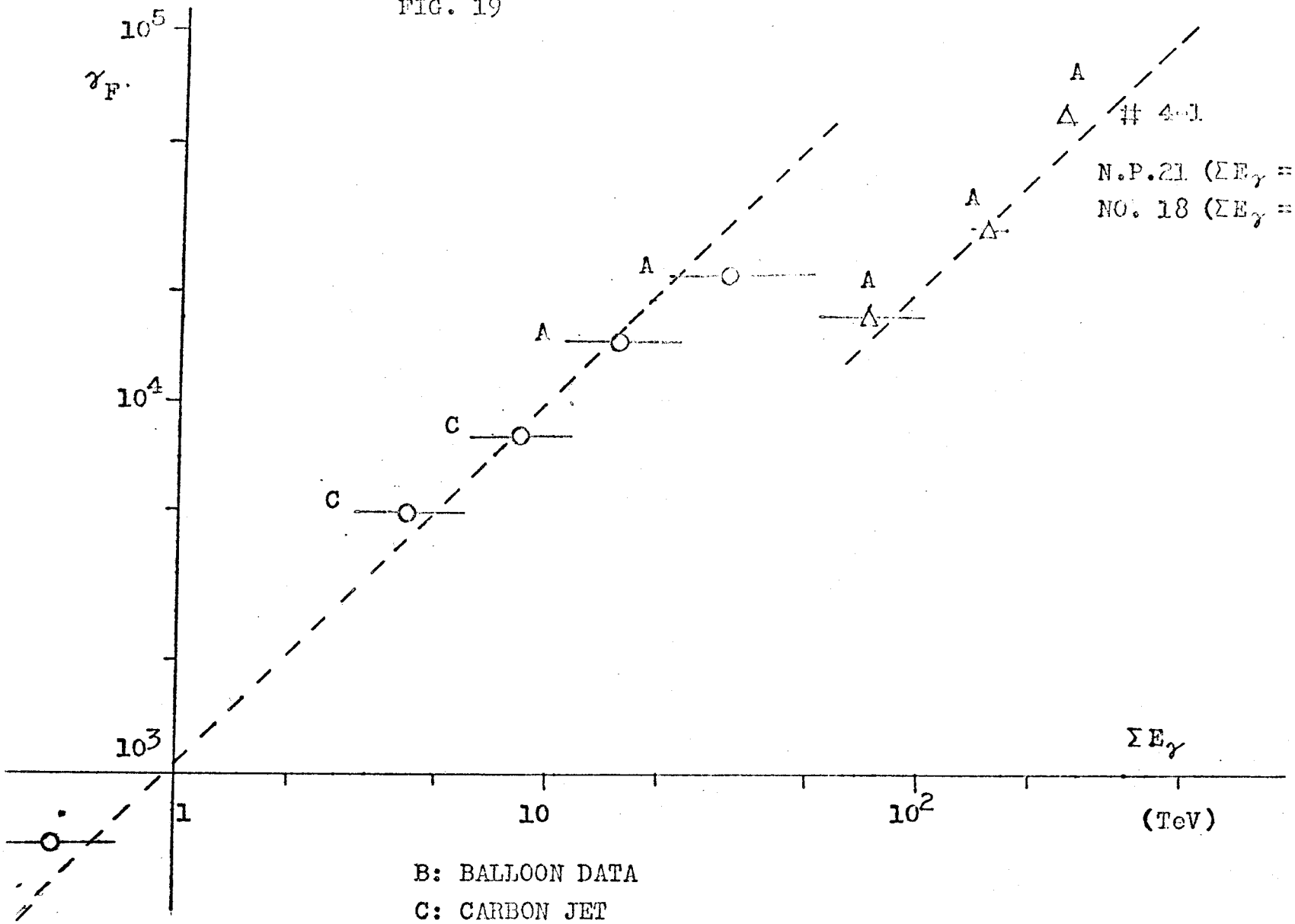
10^5
γ_F
10^4
10^3
1
10
10^2
ΣE_γ
(TeV)
A
A
A
A
C
C
N.P.21 (ΣE_γ = 142)
NO. 18 (ΣE_γ = 160)
B: BALLOON DATA
C: CARBON JET
A: ATMOSPHERIC INT

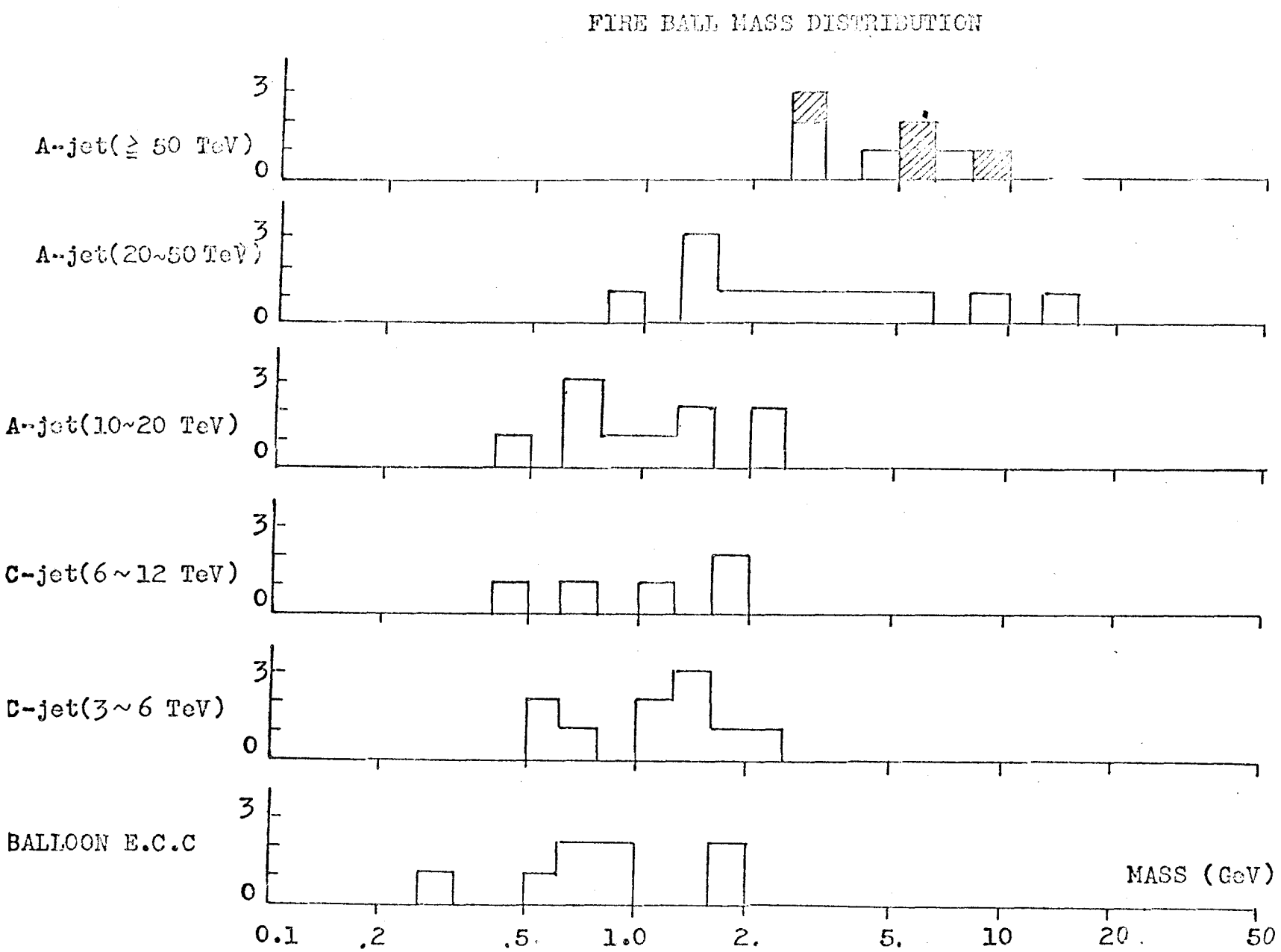
FIRE BALL MASS DISTRIBUTION
A-jet(≧ 50 TeV)
A-jet(20~50 TeV)
A-jet(10~20 TeV)
C-jet(6~12 TeV)
C-jet(3~6 TeV)
BALLOON E.C.C
3
0
MASS (GeV)
0.1
.2
.5
1.0
2.
5.
10
20
50

FIG. 20

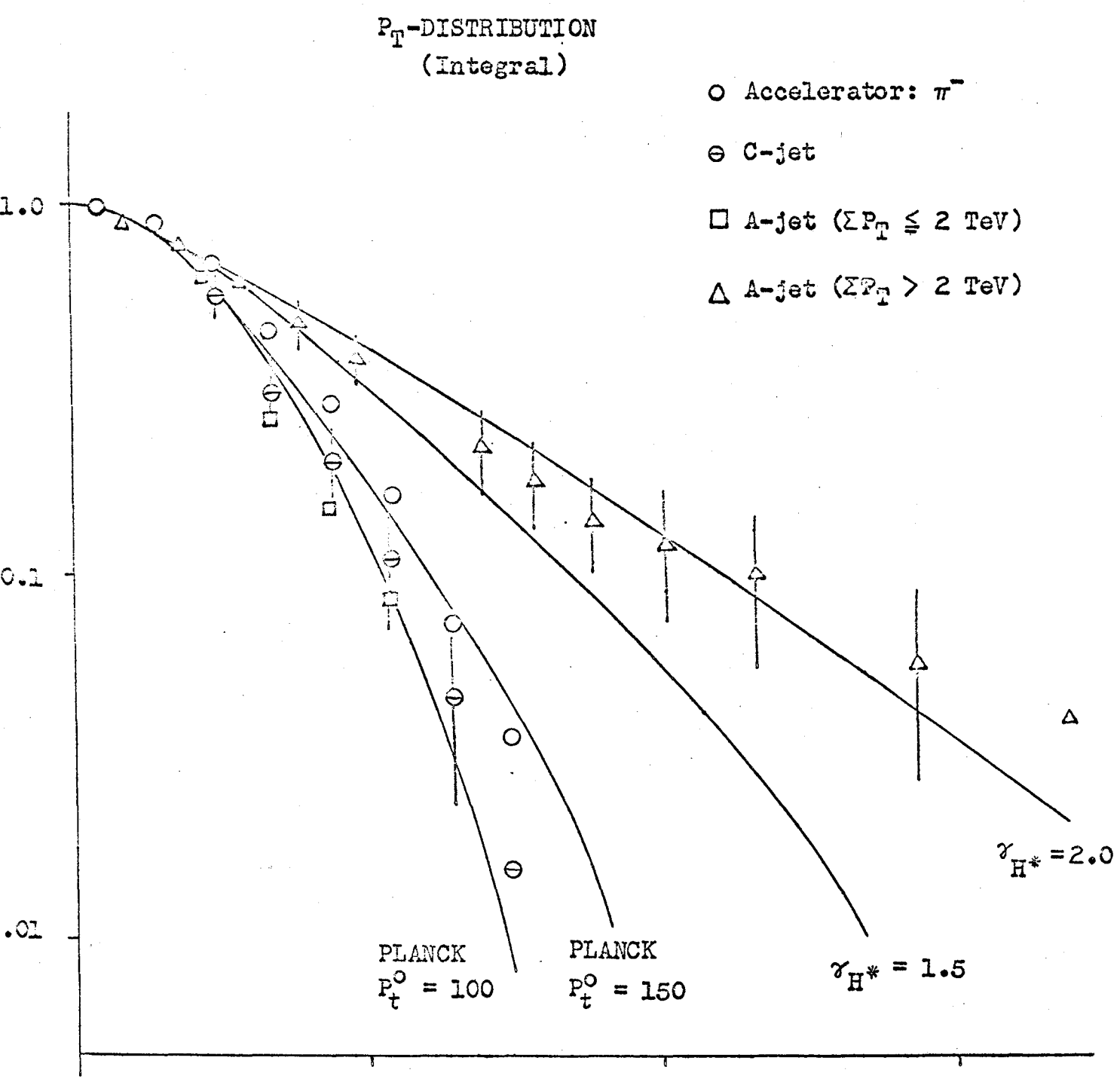
P_T-DISTRIBUTION
(Integral)
○ Accelerator: π^-
⊖ C-jet
□ A-jet ($\Sigma P_T \leqq 2$ TeV)
△ A-jet ($\Sigma P_T > 2$ TeV)
1.0
0.1
.01
PLANCK
$P_t^o = 100$
PLANCK
$P_t^o = 150$
$\gamma_{H^*} = 1.5$
$\gamma_{H^*} = 2.0$

FIG. 21

SCHEMATIC FIGURE OF EVENT 18-I

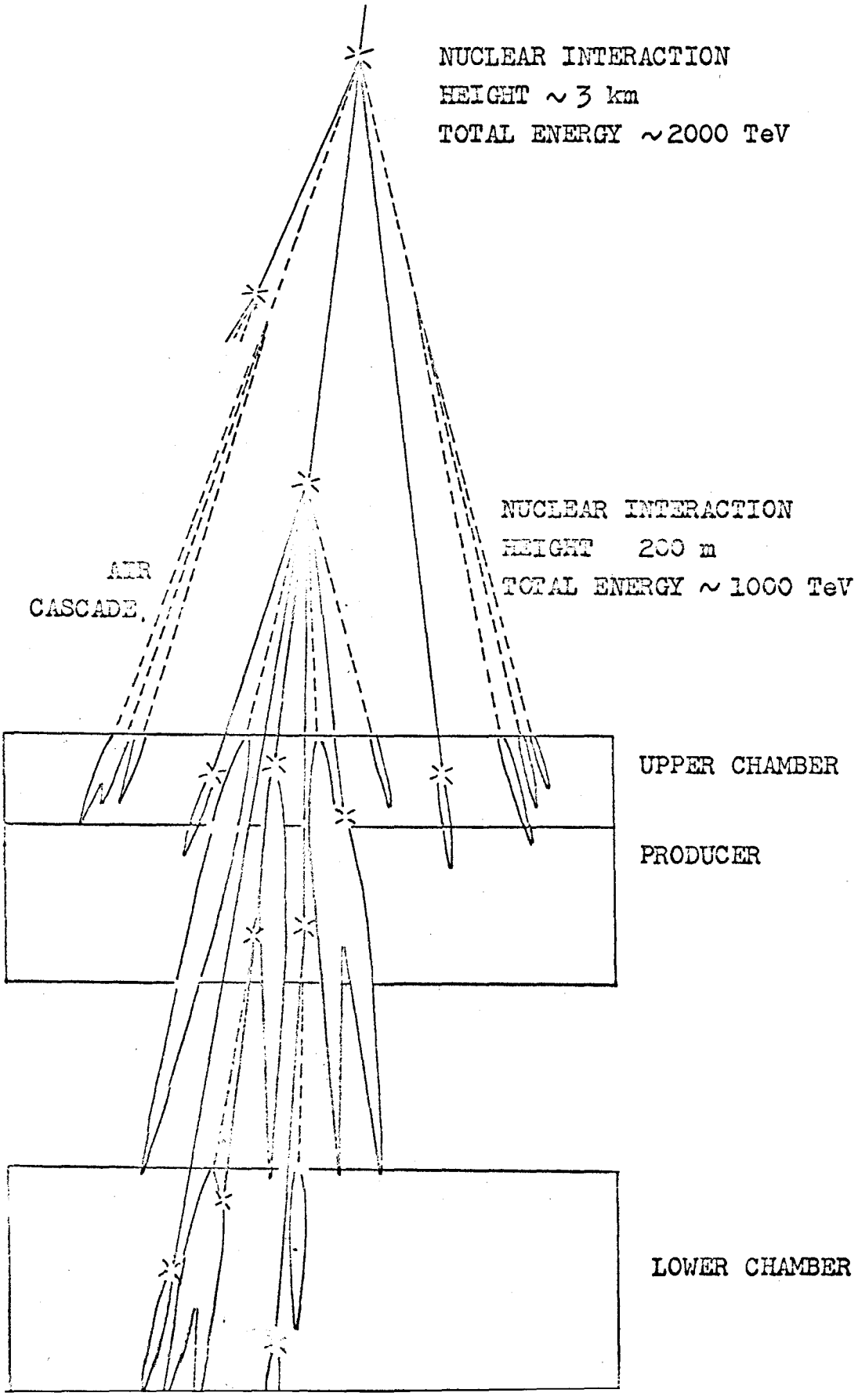

EVENT 18 · I UPPER CHAMBER FIG. 23a

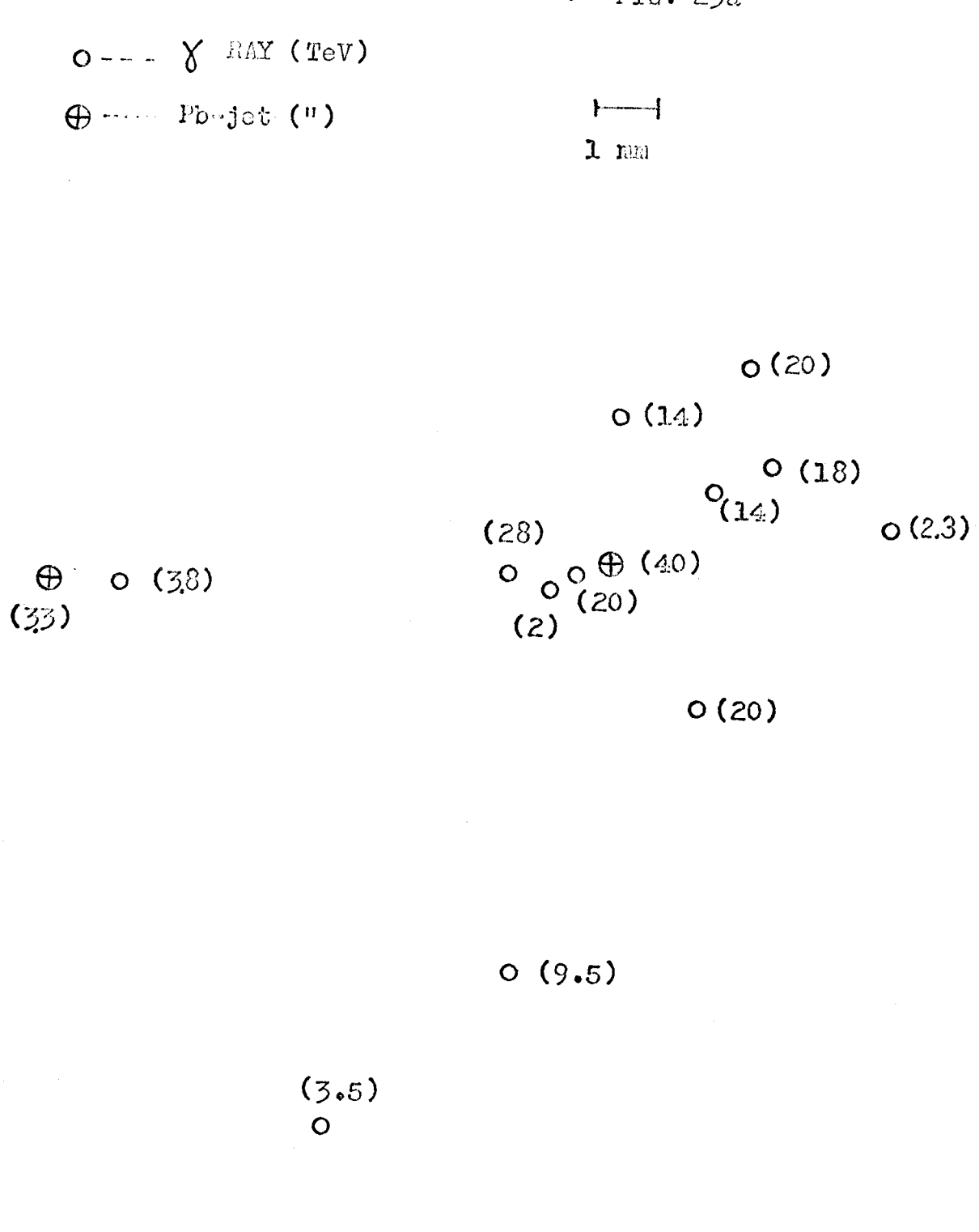

FIG. 23b

EVENT 18-I UPPER CHAMBER

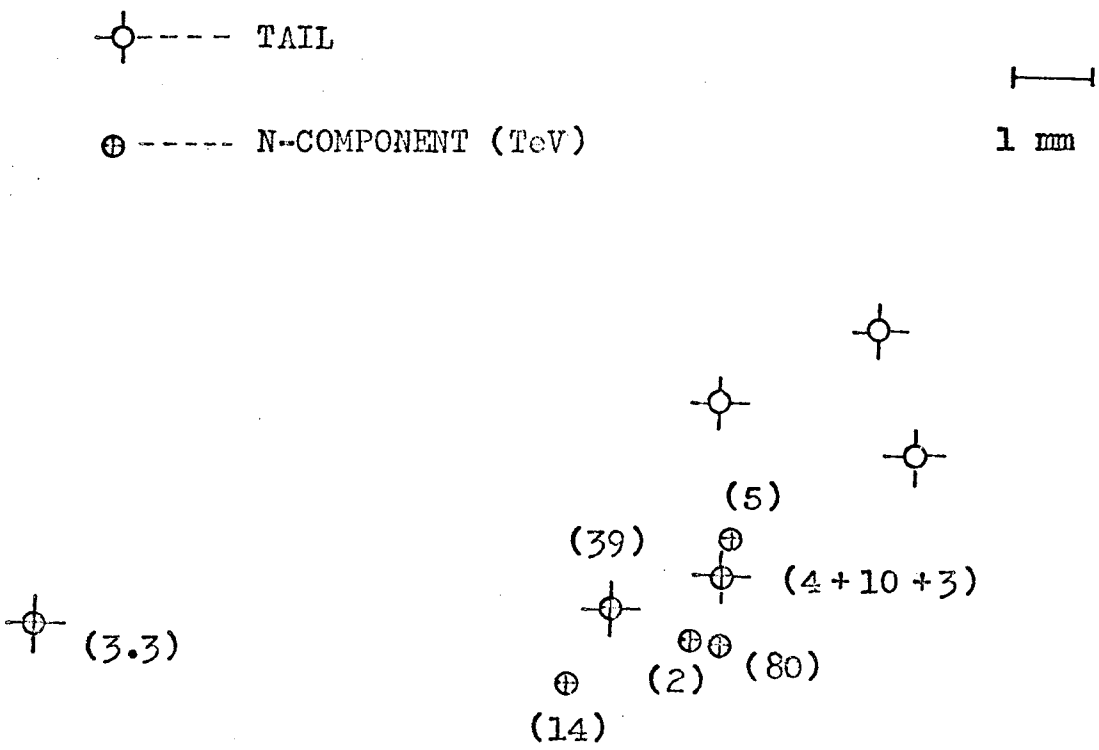

EVENT 18-1

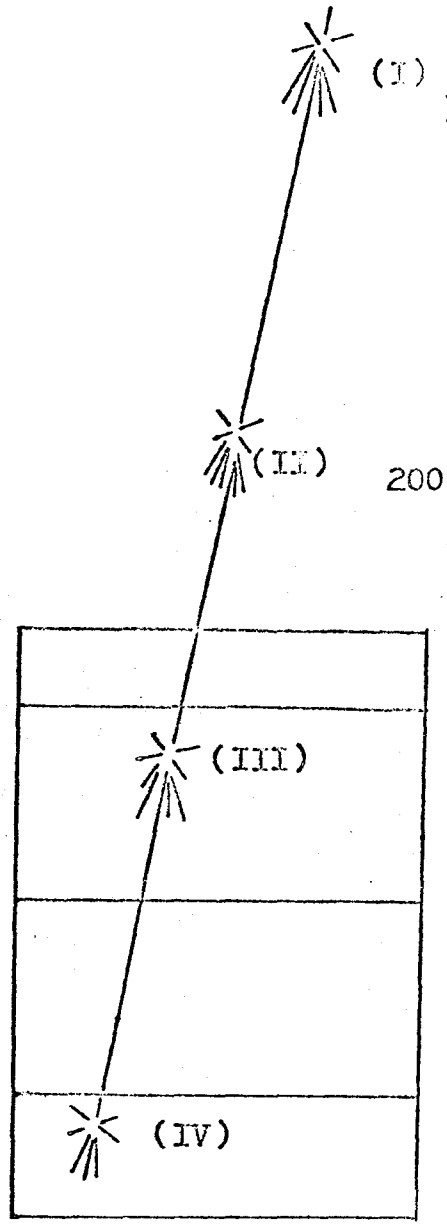

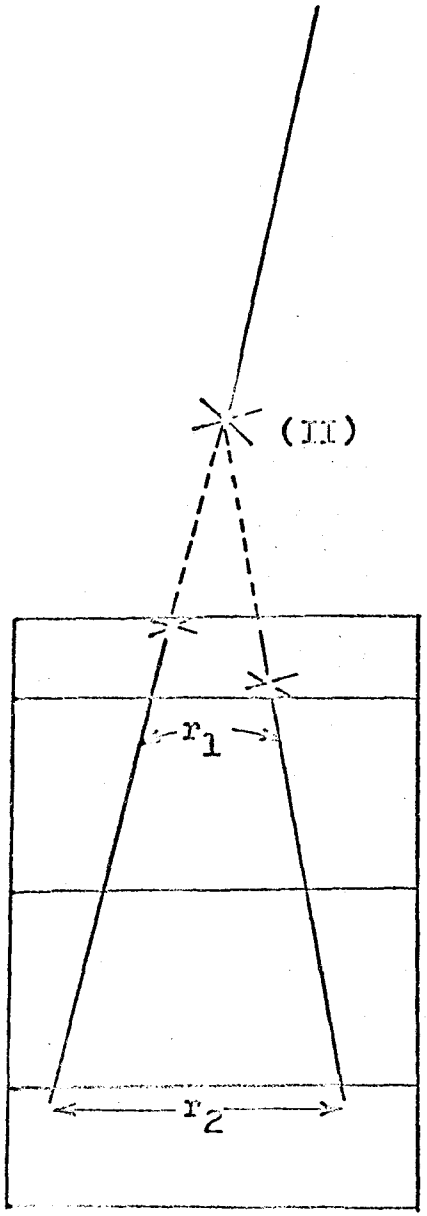

FIG. 24

$r_1 = 8817\,\mu$

$r_2 = 8998\,\mu$

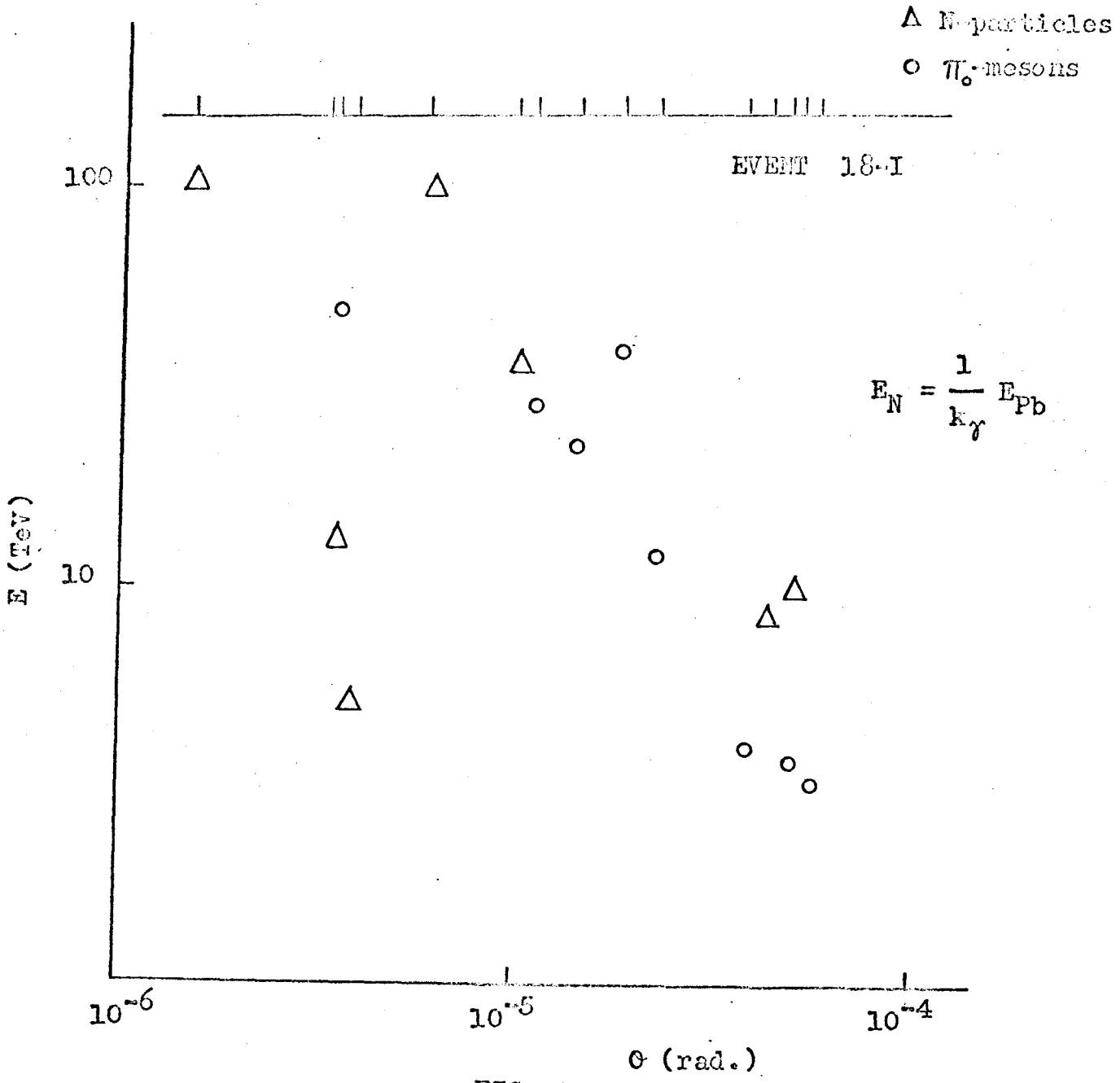
Δ N-particles
o π_o-mesons
EVENT 18-I
100
10
E (Tev)
$E_N = \frac{1}{k_\gamma} E_{Pb}$
10^{-6}
10^{-5}
10^{-4}
θ (rad.)

FIG. 25

REFERENCES:

1. There are some events showing diffuse shower spreading over a large area, particularly in the upper part of the lower chamber. They are tails of the events happened in the upper chamber. Some of them can be traced back into the nuclear plates of the upper chamber. In this way, one can make detailed geometrical correspondence between the both chambers.

2. Japanese and Brazilian Emulsion Chamber Group, The Proceedings of the International Conference on Cosmic Rays, London, 1965, Vol. 2, 744, 835, 878.

3. Akashi et al., Prog. Theor. Phys. Supple. 32 (1964), 1.

4. S. Hasegawa, Prog. Theor. Phys. 26 (1961), 151.

5. For the analysis, events including γ-rays with energy lower than $\frac{1}{10} E_{\pi_0 \text{ max}}$ are used.

6. The magnitude of the deflection due to the multiple scattering is estimated by the Monte Carlo method of three dimensional cascade theory, and it is shown to be sufficiently smaller than difference between r_1 and r_2 (see later).